Counterion-induced entropic interactions in solutions of strongly stretched, osmotic polyelectrolyte stars

A. Jusufi, C. N. Likos,[a)] and H. Löwen
Institut für Theoretische Physik II, Heinrich-Heine-Universität Düsseldorf,
Universitätsstraße 1, D-40225 Düsseldorf, Germany

We examine the conformations and effective interactions of star-branched polyelectrolytes with and without added salt, by employing monomer-resolved molecular dynamics simulations and an analytical theory. The simulations take into account the excluded-volume and Coulomb interactions between the individual monomers, as well as the counter- and coions. The theory is based on a variational free energy that is written as a sum of electrostatic, polymer, and entropic contributions of the counter- and coions. For the conformations of isolated polyelectrolyte stars, we find strong stretching of the chains, resulting in a linear scaling of the star radius with the degree of polymerization, as well as trapping and condensation of a large fraction of counterions. The effective interactions at arbitrarily strong overlaps between the stars are shown to be dominated by the entropic contributions of the trapped counterions, with the electrostatic contribution playing only a minor role due to an almost complete neutralization of the stars. In the case of added salt, we find a shrinking of the star size as well as a weakening of the effective force due to a generalized depletion mechanism. The good agreement between theory and simulations allows us to put forward analytic expressions for the effective interaction between polyelectrolyte stars at arbitrary separations. © *2002 American Institute of Physics.* [DOI: 10.1063/1.1480007]

I. INTRODUCTION

Polyelectrolytes (PEs) are polymer chains carrying ionizable groups along their backbone. Upon solution into a polar (aqueous) solvent, these groups dissociate into the solvent, leaving behind a charged polymer in coexistence with its dissolved counterions. The problem of the structure of PE solutions is a challenging one from the theoretical point of view, because it combines the complexities of polymer physics, chain connectivity and self-avoidance, and of the long-range Coulomb interaction between the charged monomers. At the same time, there exists vivid interest on these molecules, due to their numerous biological and technological applications. Typical PE biomolecules are DNA and proteins; sulfonated polysterene and polyacrylic acid, the key ingredient in diapers, are some of the most common commercially used polyelectrolytes. The structure of PE solutions, the conformational properties of the constituent macromolecules in the same, as well as the questions of counterion condensation and chain collapse have been the subject of many recent investigations[1–12] employing a variety of theoretical and computational approaches.[13]

When polyelectrolytes are grafted on surfaces they form a polyelectrolyte brush. Considerable progress toward a theoretical understanding of the properties of *planar* brushes has been made through the use of scaling theory, self-consistent field (SCF) calculations, and computer simulations.[14–18] Much less is known about spherical PE brushes. These result by grafting PEs of contour length L on

spherical colloidal particles of radius b. In the limit $L \gg b$, one obtains the star-branched polyelectrolytes or simply PE stars. These are systems of great physical and practical importance: grafting of PE chains on colloidal particles dissolved in polar solvents greatly enhances their stability against flocculation;[19,20] PE brushes are models of block co-polymer micelles formed by hydrophobically modified PEs in aqueous solutions;[21] and they have considerable potential in industrial applications due to the increased need for water-supported systems.[22,23] Pincus was the first to present a theory on the interactions of PE stars, based on scaling ideas.[19] The two fundamental ingredients in Pincus' approach are the retraction of the chains of the stars as they approach each other (no interdigitation) and the domination of the force acting between them by the entropic contribution of the trapped counterions. PE stars that have the property of absorbing most of the counterions are called *osmotic*.[24] Based on these assumptions, Pincus predicted that the force between two PE stars should be independent of their separation. Klein Wolterink *et al.*[21] and Borisov and Zhulina[24,25] put forward a scaling theory, together with SCF calculations to study the conformations of isolated PE stars.

In a recent letter,[26] we proposed an analytical theory for the conformations and interactions of PE stars and compared its predictions with the results from molecular dynamics (MD) computer simulations. In this paper, we give a detailed account of the theoretical model, which is valid for both isolated and interacting stars, and present more extensive comparisons with simulations for both salt-free and salt-containing solutions. We have investigated the sizes, conformations and interactions of PE stars for high charging frac-

tions $\alpha \geqslant 1/6$. We find a stretching of the chains and significant counterion condensation. For the force between two stars, our results are quantitatively different than the early predictions of Ref. 19, in that we find the force to be dependent on the star–star separations. Qualitatively, however, we confirm Pincus' prediction,[19] stating that the interaction is dominated by the entropic effects of the counterions and not by the electrostatic contribution. Simple, analytical expressions for the effective interactions between PE stars for given arm numbers and charging fractions are also put forward.

The rest of the paper is organized as follows: In Sec. II we examine the conformations of isolated stars, and in particular in Sec. II A we introduce the simulation model. In Sec. II B we discuss the obtained density profiles from simulations, which are used as input to the theory presented in Sec. II C. The conformations of PE stars with added salt are discussed in Sec. II D. In Sec. III we turn our attention to the effective interactions between two PE stars. The theory is presented in Sec. III A, and the results and comparisons to simulations in Sec. III B for the salt-free case and in Sec. III C for the case of added salt. In Sec. IV we summarize and conclude. As the theoretical model involves the calculation of electrostatic potentials for unusual geometries, we present this technical part in Appendixes A and B.

II. THE DILUTE LIMIT: SIZES AND CONFORMATIONS OF ISOLATED POLYELECTROLYTE STARS

A. The simulation model

We begin with the description of the simulation model, valid for both a single star polyelectrolyte and two star polyelectrolytes. We performed monomer-resolved MD simulations using the model of Stevens and Kremer,[27] Grest et al.,[28] and Grest[29] for single polyelectrolyte chains. In our considerations we have f chains with N monomers per chain, all chains coupled at a common core, whose size R_d is much smaller than the extension of the star-shaped macromolecule. The introduction of the core is necessary to accommodate the chains close to the center, where the monomer density is high.

The polyelectrolyte chains are modeled as bead-spring chains of Lennard-Jones (LJ) particles. The idea of this method was first applied on neutral linear polymers and on a single star polymer.[28,29] For good solvent conditions, a shifted LJ potential is used to describe the purely repulsive excluded volume interaction between all Nf monomers:

$$V_{LJ}(r) = \begin{cases} 4\varepsilon_{LJ}\left[\left(\dfrac{\sigma_{LJ}}{r}\right)^{12} - \left(\dfrac{\sigma_{LJ}}{r}\right)^6 + \dfrac{1}{4}\right] & \text{for } r \leqslant 2^{1/6}\sigma_{LJ}; \\ 0 & \text{for } r > 2^{1/6}\sigma_{LJ}. \end{cases}$$
(1)

Here, r is the distance of the interacting beads, σ_{LJ} is the microscopic length scale of the beads and ε_{LJ} sets the energy scale. In accordance with previous work,[30] we have chosen for the temperature $T = 1.2\varepsilon_{LJ}/k_B$, where k_B is the Boltzmann constant.

The connectivity of the bonded monomers is assured by a finite extension nonlinear elastic (FENE) potential:

$$V_{FENE}(r) = \begin{cases} -\dfrac{1}{2}k_{FENE}\left(\dfrac{R_0}{\sigma_{LJ}}\right)^2 \ln\left[1-\left(\dfrac{r}{R_0}\right)^2\right] & \text{for } r \leqslant R_0; \\ \infty & \text{for } r > R_0, \end{cases}$$
(2)

where k_{FENE} denotes the spring constant and is set to $k_{FENE} = 7.0\varepsilon_{LJ}$. This interaction diverges at $r = R_0$, which determines the maximal relative displacement of two neighboring beads. The energy ε_{LJ} is the same as in Eq. (1), whereas for the length scale R_0 we have chosen the value $R_0 = 2.0\sigma_{LJ}$.

The interactions between the monomers and the central particle mentioned above are modeled as follows: All monomers have a repulsive interaction $V_{LJ}^c(r)$ of the truncated and shifted LJ type with the central particle

$$V_{LJ}^c(r) = \begin{cases} \infty & \text{for } r \leqslant R_d; \\ V_{LJ}(r-R_d) & \text{for } r > R_d, \end{cases}$$
(3)

whereas the innermost monomers in the chain experience an additional attractive potential $V_{FENE}^c(r)$ of the FENE type with this chain, namely

$$V_{FENE}^c(r) = \begin{cases} \infty & \text{for } r \leqslant R_d; \\ V_{FENE}(r-R_d) & \text{for } r > R_d. \end{cases}$$
(4)

Each chain is charged by a fraction α in a periodical manner: every $1/\alpha$ bead carries a monovalent charge. For reasons of electroneutrality, the same amount of monovalent charges as the charged monomers, namely the $N_c = \alpha f N$ released counterions, are included in the simulation box. They are able to freely move in the box, thereby they are simulated explicitly. The snapshot shown in Fig. 1 illustrates the different kinds of particles in the system.

The full Coulomb interaction $V_{Coul}(r)$ between all charged units (monomer ions and counterions) has finally to be taken into account:

$$V_{Coul}(r_{ij}) = \frac{q_i q_j e^2}{\epsilon r_{ij}} \equiv k_B T \lambda_B \frac{q_i q_j}{r_{ij}},$$
(5)

where $q_i = \pm 1$ for the charged monomers and the counterions, respectively. The Bjerrum length λ_B is defined as the length at which the electrostatic energy equals the thermal energy

$$\lambda_B = \frac{e^2}{\epsilon k_B T},$$
(6)

where e is the unit charge of the interacting particles, and ϵ the permittivity of the solvent. For water in room temperature one obtains $\lambda_B = 7.1$ Å. Unless explicitly mentioned, no salt is added. The solvent is only taken into account via the dielectric background ϵ. The Bjerrum length is fixed to $\lambda_B = 3.0\sigma_{LJ}$. This is a realistic value for typical polyelectrolytes, such as the hydrophobic sodium poly(styrene-*co*-styrene sulfonate) or the hydrophilic poly(acrylamide-*co*-sodium-2-acrylamido-2-methylpropane-sulfonate).[31] The long-ranged Coulomb forces are calculated by the Lekner method.[32]

The single polyelectrolyte star was simulated in a cubic box with a typical edge length of $L_b = 90\sigma_{LJ}$ with periodic boundary conditions, emulating a dilute PE-star solution.
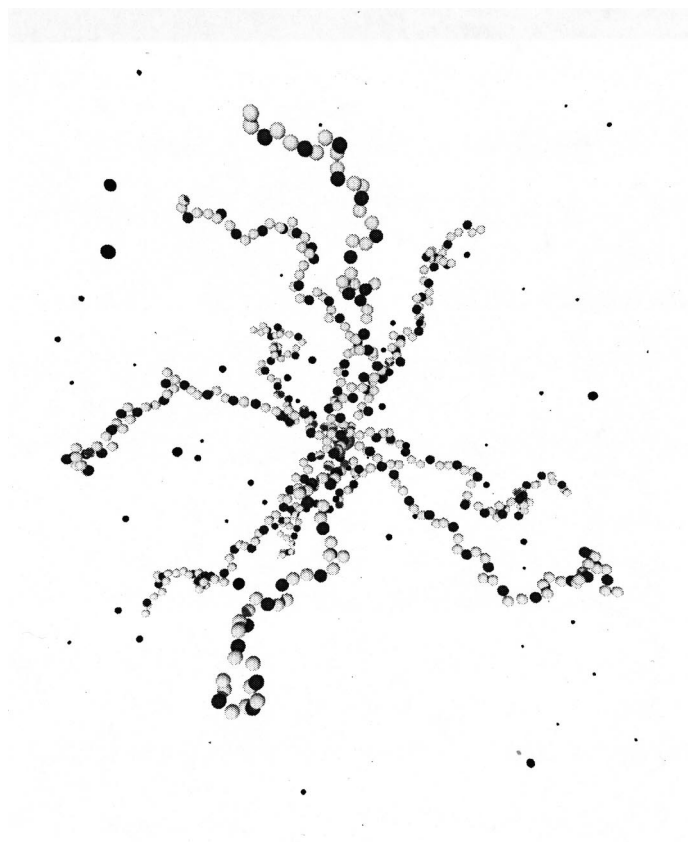
FIG. 1. Snapshot of a star-branched polyelectrolyte with $f=10$, $N=50$ and $\alpha=1/3$. The bright gray balls are the neutral monomers, and the dark spheres along the chains indicate the charged monomers (every third ball). The counterions are the small, dark spheres around the star.

The box size was varied as well, in order to investigate the influence of the long-ranged Coulomb forces and of the density on the single-star conformations. The core of the star was located at the box center and remained fixed during the simulation run. The time step was typically $\Delta t = 0.002\tau$ with $\tau = \sqrt{m\sigma_{LJ}^2/\varepsilon_{LJ}}$ being the associated time unit and m the monomer mass. The counterions were taken to have the same mass and size as the charged monomers.

After a long equilibration time (150 000–200 000 time steps), different static quantities were calculated during simulation runs lasting between 500 000 and 1 300 000 time steps, namely the center-to-end distances R and the density profiles of the monomers, the monomer ions, and the counterions that are trapped within the star due to the attractive Coulomb interaction between them and the monomer ions. Simulations were carried out for a variety of arm numbers f ($f = 5$, 10, 18, 30, 40, 50) and charge fractions α ($\alpha = 1/6$, 1/4, 1/3), allowing us to make systematic predictions for the f and α dependencies of all theoretical parameters. In addition, we investigated the chain length dependence by varying the degree of polymerization N of the chains. The values $N = 50$, 100, 150, and 200 were considered.

B. The density profile

Let $c_{mon}(r)$, $c_{charge}(r)$ and $c_{counter}(r)$ be the expectation values of the one-particle densities of the monomers, charged
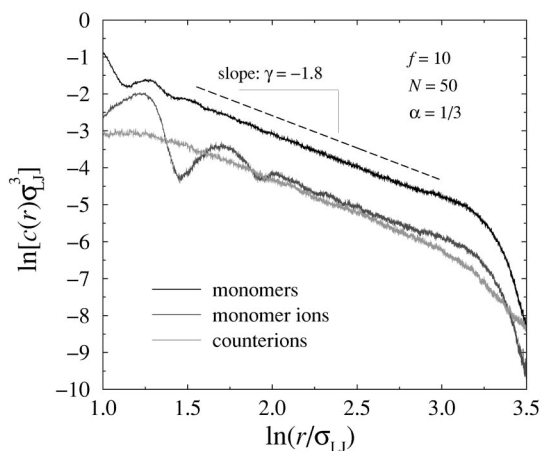

FIG. 2. Double-logarithmic plot of the density profile of monomers, monomer ions, and counterions, for a star with $f=10$, $N=50$ and $\alpha=1/3$. The slope of the scaling regime is also shown. Its value, $\gamma = -1.8$ indicates the stretching of the chains.

monomers and counterions as functions of the distance from the star center r, respectively. We measured all three quantities during the simulation run and investigated primarily their f and α dependence. In addition, we measured the fraction of trapped counterions that were condensed along the rods by surrounding every charged monomer with a fictitious sphere of radius λ_B and monitoring the number of counterions inside all spheres.

We focus here on the density profiles. As seen in Fig. 2, the monomers show a scaling behavior of their profile, a feature qualitatively similar to neutral star polymers.[30,33] Quantitatively, however, the scaling exponent is different: in the neutral-star case, one obtains $c(r) \sim r^{-4/3}$,[28,29,33] in the charged-star case we obtain a power-law $c(r) \sim r^{-1.8}$, i.e., the chains are much more stretched. To demonstrate this point, we show in Fig. 3 snapshots of a charged and a neutral star; the stretching of the chains of the charged star is manifest.
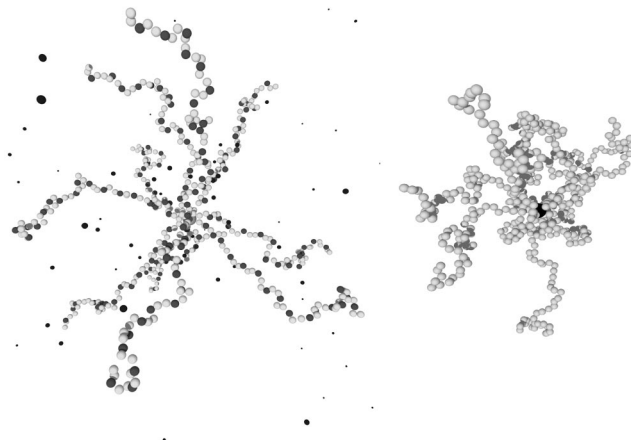

FIG. 3. Snapshots of a polyelectrolyte star (left picture, $\alpha=1/3$) and a neutral star polymer (right picture, $\alpha=0$) each with $f=10$ arms and $N=50$ monomers per arm. The stretching of the chains in the case of the charged star, in contrast to the neutral star, can be clearly seen.

11014   J. Chem. Phys., Vol. 116, No. 24, 22 June 2002
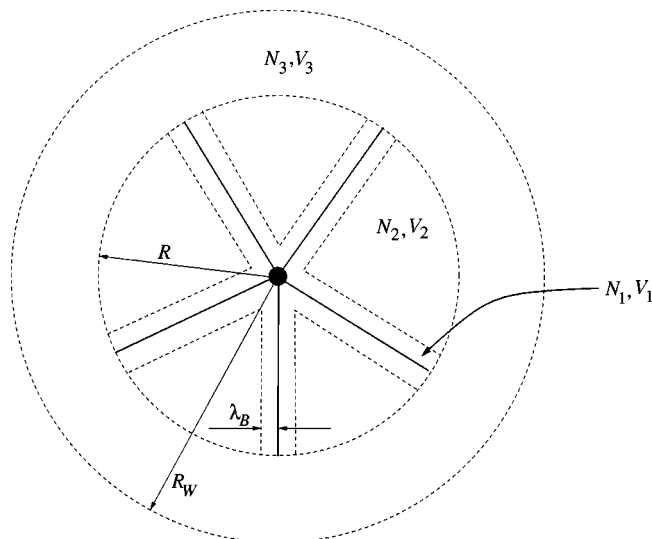
Jusufi, Likos, and Löwen

FIG. 4. A sketch of a polyelectrolyte star in its spherical Wigner–Seitz cell. For demonstration, five chains (solid lines) are assumed to be fully stretched and are surrounded by cylinders (dashed lines) where the condensed counterions are located. For further explanations, see text.

The fully rodlike chain limit yields a monomer profile scaling as[24,25] $c(r) \sim r^{-2}$ and hence a slope -2 in a double-logarithmic plot. This rodlike behavior has been experimentally observed in neutron scattering studies of block copolymer micelles.[34] Because of small lateral fluctuations of the chains,[8,9] the fully rodlike limit is not reached here and the slope $\gamma = -1.8$ is obtained.[35] Nevertheless, the value indicates an almost complete stretching of the chains. The counterion density profile shows the same scaling as that of the monomers. This is a manifestation of the tendency of the counterions to achieve local charge neutrality, a feature also seen in simulations of planar polyelectrolyte brushes.[17] However, the counterions, in contrast to the monomers, are not bounded and therefore they add a high entropic contribution to the free energy of the system. This is a relevant point because many investigations on these systems are based on homogeneous distributions of the counterions within PE-star

TABLE I. Comparison of conformational properties between simulation and theory for different arm numbers f. The chain length is fixed to $N=50$, and the cell radius is $R_W = 55.83\ \sigma_{LJ}$, except for $f=40$ ($R_W = 62.04\ \sigma_{LJ}$), and $f=50$ ($R_W = 74.44\ \sigma_{LJ}$).

f	α	N_c	$(R/\sigma_{LJ})^a$	$(R/\sigma_{LJ})^b$	$(N_{in})^a$	$(N_{in})^b$	$(N_1)^a$	$(N_1)^b$
5[c]	1/3	80	26.8	26.1	47	57	27	25
10[c]	1/6	80	23.4	23.7	42	59	22	38
10[c]	1/4	120	25.3	25.2	77	97	46	61
10[c]	1/3	160	27.4	26.9	110	134	72	81
18[c]	1/6	144	24.2	25.8	91	121	60	90
18[c]	1/4	216	26.6	26.9	156	190	107	141
18[c]	1/3	288	28.3	28.1	217	260	159	190
30	1/4	360	27.2	28.8	278	332	213	272
30	1/3	480	28.6	29.7	384	449	309	366
40	1/3	640	29.2	30.9	531	607	392	517
50	1/3	800	29.8	32.0	668	763	514	670

[a]Simulation.
[b]Theory.
[c]From Ref. 26.

TABLE II. Comparison of the conformational properties obtained from simulation and theory for different chain lengths N. Here the arm number is fixed to $f=10$, the charge fraction is $\alpha \simeq 1/3$, and the cell radius is $R_W = 55.83\ \sigma_{LJ}$ for $N=50$ and $R_W = 136.48\ \sigma_{LJ}$ for all other chain lengths.

N	N_c	$(R/\sigma_{LJ})^a$	$(R/\sigma_{LJ})^b$	$(N_{in})^a$	$(N_{in})^b$	$(N_1)^a$	$(N_1)^b$
50	160	27.4	26.9	110	134	72	81
100	330	57.3	54.0	236	269	96	103
150	500	84.2	78.8	382	420	131	133
200	660	106.7	100.4	553	572	169	162

[a]Simulation.
[b]Theory.

polyelectrolytes.[21,24,25,36] As we will see in Sec. III, the inhomogeneous behavior of the counterions play a crucial role for the effective interaction between two polyelectrolyte stars.

C. Theory of isolated polyelectrolyte-stars

In the theoretical investigations, we employ a mean-field, Flory-type approach for the analysis of the large-scale properties of polyelectrolyte stars, which is akin to that of Ref. 21. We consider a star in a dilute solution of density $\rho_{st} = N_{st}/V$ containing N_{st} PE stars in the macroscopic volume V. We define accordingly the Wigner–Seitz radius (or ion-sphere radius) $R_W = (4\pi \rho_{st}/3)^{-1/3}$. The star is envisioned as a sphere of radius R enclosed in a cell of radius $R_W > R$; all counterions are restricted to move inside this cell. Figure 4 illustrates the situation and is helpful for further considerations.

Particular attention has to be paid to the Manning condensation of counterions on the rodlike chains.[5,7,37–40] The condensation takes place when the dimensionless parameter $\xi = \lambda_B N\alpha/R$ exceeds unity.[38] This condition is satisfied for all our parameter combinations, see Tables I–III. Thus, in the model, the N_c counterions are partitioned into three different states: N_1 *condensed* counterions within f tubes around the branches of the star: these are confined to move in quasi-one-dimensional cylindrical domains. N_2 *trapped* counterions inside the star: these are allowed to explore the whole interior of the star. Finally, N_3 *free* counterions that move into the

TABLE III. Comparison of the conformational properties between simulation and theory for two different chain numbers f and different salt concentrations c_s. The charge fraction is fixed to $\alpha \simeq 1/3$, and the cell radius is $R_W = 55.83\ \sigma_{LJ}$.

f	N_c	N_s	c_s (mol/lt)	$(R/\sigma_{LJ})^a$	$(R/\sigma_{LJ})^b$	$(N_{in})^a$	$(N_{in})^b$	$(N_1)^a$	$(N_1)^b$
5	80	250	0.036	22.1	22.2	73	73	40	22
5	80	600	0.088	20.7	19.4	87	76	44	29
10	160	250	0.036	24.0	25.0	138	150	81	60
10[c]	160	600	0.088	22.6	22.7	156	155	90[d]	71
10[c]	160	750	0.109	21.8	22.1	164	156	95[d]	74
10	160	1000	0.146	21.9	21.3	173	156	98	74

[a]Simulation.
[b]Theory.
[c]From Ref. 26.
[d]These entries were erroneous in Ref. 26 due to a programming error. We quote here the correct results.

bulk of the solution and in the model they are located in the region $R < r < R_W$. This approach is similar to the three-state model of Kramarenko et al.,[41] employed for polyelectrolyte microgel particles. To specify the available volumes to the condensed and trapped counterions, we introduce tubes of length R and radius λ_B surrounding each rod, and treat all counterions contained in these tubes as condensed. Thus, the interior volume $V(R) = 4\pi R^3/3$ of the star is divided as $V(R) = V_1 + V_2 + f\pi\sigma_{LJ}^2 R$ with $V_1 = f\pi(\lambda_B^2 - \sigma_{LJ}^2)R$ being the total volume of the hollow tubes, available to the condensed counterions, and V_2 the volume remaining available to the N_2 trapped counterions inside. Moreover, let $V_3 = 4\pi(R_W^3 - R^3)/3$ be the volume of the spherical shell for the free counterions, and $\rho_i(r)$, $i = 1,2,3$, the *number* densities of the three counterion types. Clearly, the number of free counterions N_3 is equal to the number of the uncompensated charges of the star Q^*/e. We emphasize that all counterions are indistinguishable particles and have been treated in this way in all considerations to follow. Particle exchanges between the three possible states constantly take place and the numbers N_i, $i = 1,2,3$ are simply expectation values and not prescribed occupation numbers of counterions that have been "marked" to belong to one state or the other.

The equilibrium values for R and N_i are determined through minimization of a variational free energy which we write as

$$\mathcal{F}(R,\{N_i\}) = U_H + U_c + F_{el} + F_{Fl} + \sum_{i=1}^{3} S_i, \tag{7}$$

where U_H and U_c are electrostatic contributions, F_{el} and F_{Fl} elastic and self-avoidance contributions from the chains and S_i entropic contributions from the counterions, to be described in detail in what follows.

The term U_H is the Hartree-type, mean-field electrostatic energy of the whole star

$$U_H = \frac{1}{2\epsilon} \int\int d^3r \, d^3r' \frac{\varrho(\mathbf{r})\varrho(\mathbf{r}')}{|\mathbf{r}-\mathbf{r}'|}, \tag{8}$$

with the local *charge* density $\varrho(\mathbf{r})$ to be defined below. The only relevant correlations arise between the condensed counterions and the charges on the chains because the average density of the trapped counterions is very low. Hence, the correlation energy U_c stems from the attractions between the rods and the condensed counterions contained in the associated tubes. To estimate the average rod-condensed counterion separation z_m, we take $z_m = (1/2)\sqrt{\lambda_B^2 + y_m^2}$, where $y_m = R/(N\alpha)$ is the distance between two sequential charged monomers along the chain, obtaining for the correlation energy resulting from N_1 condensed counterions:

$$\frac{U_c}{k_B T} = -\frac{\lambda_B N_1}{z_m}. \tag{9}$$

Figure 5 illustrates the chosen value for z_m resulting from geometrical considerations. The term F_{el} is the elastic contribution of the chains, written as

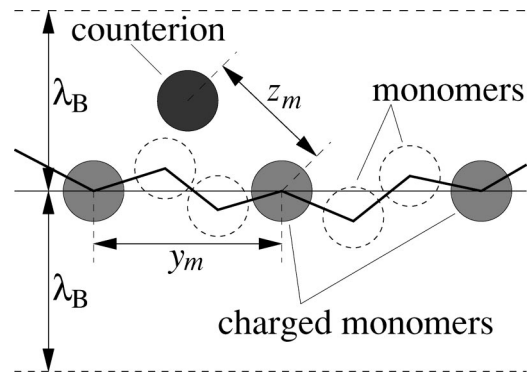$$\frac{F_{el}}{k_B T} = \frac{3 f R^2}{2 N \sigma_{LJ}^2}, \tag{10}$$

FIG. 5. A sketch of a chain segment for the case $\alpha = 1/3$, showing monomers (dashed-lined hollow spheres), charged monomers (bright gray spheres) and a counterion (dark gray sphere). The tube radius is λ_B from the central line, indicating the stretched behavior of the chain. The neutral monomers can deviate from the central line, whereas the charged monomers are situated along this line. The counterion is assumed to be placed between two charged monomers with a distance z_m to them.

and is a Gaussian approximation of the conformational entropy of the arms of the star, where we identified the monomer length with σ_{LJ}. For the nonelectrostatic contribution of the chains F_{Fl}, arising through their self-avoidance, we employ the Flory-type expression

$$\frac{F_{Fl}}{k_B T} = \frac{3 v (f N)^2}{8 \pi R^3}, \tag{11}$$

with the excluded volume parameter v. As usual for the case of good-solvent conditions, triplet-monomer contributions have been omitted. Finally, the terms S_i are ideal entropic contributions of the form

$$S_i = k_B T \int_{V_i} d^3r \, \rho_i(r) [\ln(\rho_i(r)\sigma_{LJ}^3) - 1]$$
$$+ 3 N_i \ln\left(\frac{\Lambda}{\sigma_{LJ}}\right), \tag{12}$$

with $\rho_i(r) = N_i/V_i$ being the number densities of the counterions in the three possible states. Λ is the thermal de Broglie wavelength of the counterions. In writing the sum of the three entropic contributions in Eq. (7), the last terms contribute only the trivial constant $3N_c \ln(\Lambda/\sigma_{LJ})$ which will be dropped in what follows.

We discuss the mean-field electrostatic and the entropic terms in more detail. Since the chains are modeled as being fully stretched, the density distributions inside the stars fall off as $\sim r^{-2}$ from the center but are uniform outside the star. We note that this is different from the approach of Ref. 21, where uniform densities inside *and* outside the star were employed. Though we obtained reasonable results for the isolated star using such trial profiles, the nonuniform ones are of paramount importance for obtaining agreement with simulation results regarding the effective interaction, as we will discuss shortly. Accordingly, we write

$$\frac{\varrho(\mathbf{r})}{Q^*} = \frac{\Theta(R-r)}{4\pi R r^2} - \frac{\Theta(r-R)\Theta(R_W-r)}{V_3}, \tag{13}$$

with the net charge $Q^* = |e|(N_c - N_1 - N_2) = |e|N_3$ and the Heaviside step function $\Theta(x)$. We thus obtain the electrostatic energy as

$$\frac{U_H}{k_B T} = \frac{N_3^2 \lambda_B}{2R} \vartheta\left(\frac{R}{R_W}\right), \tag{14}$$

where the function $\vartheta(x)$ is given by

$$\vartheta(x) = 1 + \frac{5 - 9x + 5x^3 - x^6}{5(1 - x^3)^2}. \tag{15}$$

In order to calculate the entropic contributions of the counterions in Eq. (12), we need to specify the number densities $\rho_i(r)$. We model the condensed counterions as having a uniform distribution inside the tubes, an assumption supported by simulation results on single PE chains having typical values of the ratios $\alpha\lambda_B/\sigma_{LJ}$ considered here.[5] Thus, $\rho_1(r) = N_1/V_1$ inside the tubes and zero otherwise. Since the trapped counterions follow the profile of the charged monomers, we take $\rho_2(r) = Cr^{-2}\Theta(R - r)$. The volume which is available for the N_2 trapped counterions inside the star is reduced by the presence of the tubes around the chains. We therefore introduce a representative sphere of radius R' having the same volume V_2 as that available to the N_2 counterions and calculate the prefactor C of ρ_2 using the normalization condition $C = N_2/(4\pi R')$. The reduced radius R' is determined by the equation

$$\frac{4\pi}{3}R^3 - f\pi\lambda_B^2 R = \frac{4\pi}{3}R'^3 \equiv V_2, \tag{16}$$

yielding

$$R' = R\left[1 - \frac{3}{4}f\left(\frac{\lambda_B}{R}\right)^2\right]^{1/3}. \tag{17}$$

Finally, we assume a uniform distribution of the free counterions within the cell $R < r < R_W$ and take $\rho_3(r) = \Theta(r - R)\Theta(R_W - r)N_3/V_3$.

Carrying out the integrations in Eq. (12), we obtain the following expressions for the entropic contributions of the counterions in their three different states:

$$\frac{S_1}{k_B T} = N_1\left[\ln\left(\frac{N_1\sigma_{LJ}^3}{V_1}\right) - 1\right], \tag{18}$$

$$\frac{S_2}{k_B T} = N_2\left[\ln\left(\frac{N_2\sigma_{LJ}^3}{4\pi R'^3}\right) + 1\right], \tag{19}$$

$$\frac{S_3}{k_B T} = N_3\left[\ln\left(\frac{N_3\sigma_{LJ}^3}{V_3}\right) - 1\right]. \tag{20}$$

The Flory term in Eq. (11) takes into account, in a mean-field fashion, the loss of entropy of the chains due to the *short-range*, steric repulsions of the monomers, through the effective, excluded-volume parameter v. The value of this parameter for stiff PEs has been the topic of extensive discussion in the literature.[15,19,39] If the chains were neutral, then a good estimate for v term would be the volume of the monomer bead, $v \cong \sigma_{LJ}^3$. The presence of the condensed counterions, though, introduces monomer pairs along the backbones of the chains, whose effective diameter is σ_{pair}

$> \sigma_{LJ}$. Since the condensed counterions are to be found in typical distances λ_B from the chain backbone, we thereby set $\sigma_{pair} = \lambda_B = 3\sigma_{LJ}$ and thereby obtain $v = \sigma_{pair}^3 \cong 30\sigma_{LJ}^3$. This is the value that we employed in all our theoretical analyses. It is also in agreement with the "screened electrostatic" estimate $v \cong \lambda_B\kappa^{-2}\alpha^2$ of Ref. 21, with $\kappa = \sqrt{3N_2\lambda_B/R^3}$, for typical values of α, N_2 and R read off from Table I.

The values R and N_i $(i = 1,2,3)$ are found by minimization of the free energy Eq. (7). The results read as

$$R^3 = \frac{N}{3f}\left\{\frac{\lambda_B\sigma_{LJ}^2 N_3^2}{2}\left[\vartheta(R/R_W) - \frac{R}{R_W}\vartheta'(R/R_W)\right]\right.$$
$$+ 3R\sigma_{LJ}^2\left[N_2\left(1 + \frac{2}{3}\frac{\pi f\lambda_B^2 R}{V_2}\right) - N_3\frac{V(R)}{V_3}\right]$$
$$\left. + N_1 R\sigma_{LJ}^2\left[1 - \left(\frac{f}{N_c}\right)^2\frac{\lambda_B R^2}{4z_m^3}\right] + \frac{9}{8\pi}\left(\frac{fN\sigma_{LJ}}{R}\right)^2 v\right\}; \tag{21}$$

$$N_3 = \frac{R}{\lambda_B\vartheta(R/R_W)}\left\{2 + \ln\left[\left(\frac{N_c - N_1}{N_3} - 1\right)\frac{V_3}{3V_2}\right]\right\}; \tag{22}$$

$$N_1 = (N_c - N_3)\left[1 + \frac{3V_2}{V_1}\exp\left(-2 - \frac{\lambda_B}{z_m}\right)\right]^{-1}, \tag{23}$$

where $\vartheta'(x) = d\vartheta/dx$. All quantities acquire an explicit density dependence through R_W, a usual situation for charged systems, familiar from the statistical mechanics of charged-stabilized colloids as well.[42] The results for different parameter combinations are shown in Tables I and II in comparison with simulation data.

Referring to Table I, in which the degree of polymerization is fixed to $N = 50$, we see that the radii values from theory and simulation are in very good agreement for all parameter combinations considered. Moreover, the radius is practically f independent, a manifestation of the fact that the chains are stretched. This is one of the features that distinguish PE stars from neutral ones, for which the scaling $R \sim f^{1/5}N^{3/5}$ holds.[30,33] As far as the total number of trapped counterions $N_{in} = N_1 + N_2$ and N_1 of condensed counterions are concerned, the following remarks can be made: both are overestimated in the theory by an amount depending on the charging fraction α. This overestimation can be explained by the fact that we assumed a complete stretching of the chains (rodlike configuration), which results in a stronger electrostatic attraction than the true one, in which lateral chain fluctuations are present. The same mechanism is responsible for the overestimation of N_1. This claim is corroborated by the remark that the largest discrepancies occur for the smallest charge fraction $\alpha = 1/6$, where the assumption of stretched chains is most questionable. On the other hand, the *ratio* of condensed to absorbed counterions appears to be almost constant, $\sim 70\%$ for all combinations considered, both in theory and simulation. With our present, minimal assumptions, we find that the theory captures quantitatively all features of the star conformations. It reproduces the tendency of the PE stars

to increase the fraction $N_{\rm in}/N_c$ of absorbed counterions as f and/or α increase, in line with the predictions of scaling theory in the "osmotic star" regime.[24,25]

In Table II we show the results obtained for fixed arm number $f=10$ and varying N. First, we observe a linear scaling of the star radius $R\sim N$, confirming the overall stretched-chain configuration. Once again, theory and simulation are in very good agreement regarding the radius values. In order to achieve good agreement for the number of condensed counterions, we had to gradually increase the value of the tube radius, though. As the chain length increases, so does the *absolute* value of the transverse chain fluctuations,[8] although the size of their *relative* fluctuations must remain bounded, so that the overall chain configuration is still stretched. This means that the range in which our model rodlike chains can capture counterions and condense them effectively increases. In order to estimate this enhanced range, we fixed the ratio μ of tube radius to chain length (the relative fluctuation) to its value for $N=50$, i.e., $\mu=\lambda_B/R(N=50)\cong 10\%$. Thereafter, we determined the tube radius $R_{\rm tube}$ through the relation $R_{\rm tube}(N)=\mu R(N)\sim\mu N$. This change of the tube radius affects the number of condensed counterions N_1 but has otherwise only a minor effect on the other two quantities R and $N_{\rm in}$.

D. An isolated star with added salt

The theory can also be extended to the case of added salt by the addition of entropic terms for the counter- and coions. With the addition of N_s salt molecules, the solution contains N_s negatively charged coions and N_s positively charged salt counterions, yielding a total number of N_c+N_s counterions in the system. The counter- and coions are separated into those absorbed in the interior of the star $N_{\rm in}^{\pm}$ and those outside: $N_{\rm out}^+=N_s+N_c-N_{\rm in}^+$ and $N_{\rm out}^-=N_s-N_{\rm in}^-$. The entropic terms of Eqs. (19) and (20) are now modified through the replacements $N_2\to N_{\rm in}^++N_{\rm in}^--N_1$ and $N_3\to 2N_s+N_c-(N_{\rm in}^+ +N_{\rm in}^-)$. With these changes, the theory for the salt-free case can now be carried over to the case of added salt, whereby one additional degree of freedom appears, namely the distribution of coions between the interior and the exterior of the star. With these modifications, the procedure remains the same and the conformational properties are determined by the requirement of minimization of the variational free energy with respect to R, $N_{\rm in}^+$, $N_{\rm in}^-$, and N_1.

The procedure yields $N_{\rm in}^-=0$ for all cases considered, i.e., no coions penetrating the star. We have performed simulations for the salted case as well finding, in agreement with theory, that the addition of salt results in an almost complete neutralization of the PE star with increasing salt concentration c_s, to a shrinking of its radius and to an exclusion of all coions from the star interior. In Table III, we summarize the results obtained for different salt concentrations $c_s=N_s/V(R_W)$. First we note that the radius of the stars decreases with increasing salt concentration. This is caused by the increased osmotic pressure of the salt ions outside the star. The cases in which $N_{\rm in}>N_c$, seen only in the simulation results, are caused by the penetration of a small number of coions ($<5\%$ of their total number) into the star interior,
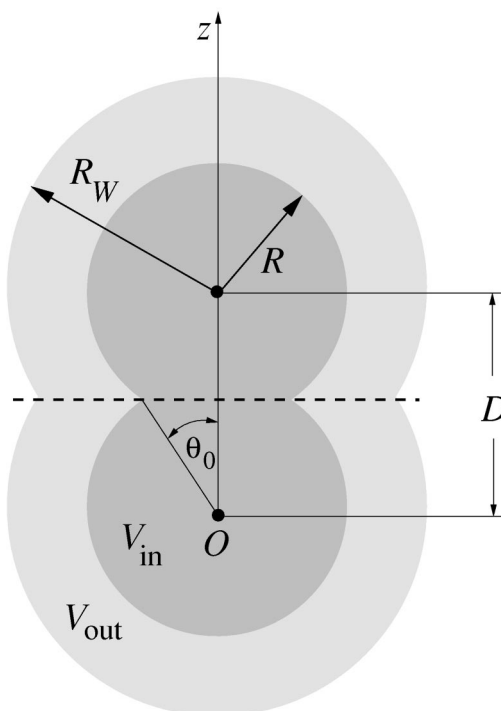

FIG. 6. A sketch of two polyelectrolyte-stars of radius R each, held at center-to-center separation D. The dark fused spheres denote the stars and have a total volume $V_{\rm in}$. The light eight-shaped hollow region with volume $V_{\rm out}$ denotes the region in which the free counterions can move.

whereas the theory predicts that no coions penetrate into the star. However, in view of the fact that in simulations only a tiny fraction of coions are found inside the star, this discrepancy appears to be insignificant. Theory and simulation are in agreement in predicting that essentially all coions remain free in the star exterior.

III. CONCENTRATED SOLUTIONS: EFFECTIVE INTERACTIONS BETWEEN STAR-BRANCHED POLYELECTROLYTES

A. Theory

The effective interaction $V_{\rm eff}(D)$ between two PE stars, kept at center-to-center distance D, results after taking a canonical trace over all but the star center degrees of freedom and is defined as

$$V_{\rm eff}(D)=\mathcal{F}_2(D)-\mathcal{F}_2(\infty),\qquad(24)$$

where $\mathcal{F}_2(z)$ is the Helmholtz free energy of two PE stars at center-to-center separation z.[43] For the theoretical investigations of the force at overlapping distances $D\leqslant 2R$, we take into consideration that, when two PE stars overlap, the chains of each star retract, a feature already conjectured by Pincus[19] and also confirmed in all simulations that we carried out. We model the two stars as "fused spheres," each carrying the cloud of its untrapped counterions around it, as shown in Fig. 6. The chains remain stretched, thus the $\sim r^{-2}$ falloff of the density profile from each star center remains. To model the chain retraction, each profile is sharply cut off

as soon as the distance from the corresponding center reaches the bisecting plane located at a distance $D/2$ from the centers.

The variational free energy $\mathcal{F}_2(D)$ is written as in Eq. (7). Since the terms U_c, F_{el} and F_{Fl} remain unaffected by D, $V_{eff}(D)$ contains only the electrostatic $U_H(D)$ and the entropic contributions $S_i(D)$, $i=1,2,3$:

$$V_{eff}(D) = U_H(D) + \sum_{i=1}^{3} S_i(D)$$

$$= \min_{\{R,\{N_i\}\}} \mathcal{F}_2(D;R,\{N_i\}). \qquad (25)$$

We first investigate the electrostatic part $U_H(D)$ in more detail. It is convenient to separate the total charge density $\varrho(\mathbf{r})$ into two contributions, $\varrho_{in}(\mathbf{r})$ in the interior of the fused spheres (V_{in}) and $\varrho_{out}(\mathbf{r})$ in the eight-shaped region outside (V_{out}). $\varrho_{out}(\mathbf{r})$ is homogeneous and equal to $-Q^*/V_{out}$. We choose a spherical polar coordinate system with its origin the center of the lower star (see Fig. 6). Setting $r_\theta = r\cos\theta$ and $\omega \equiv \theta - \theta_0$, we write

$$\varrho_{in}(\mathbf{r}) = A|e|[P(\mathbf{r}) + P(\mathbf{D} - \mathbf{r})] \qquad (26)$$

with the shape function

$$P(\mathbf{r}) = \frac{1}{r^2}[\Theta(R-r)\Theta(\omega) + \Theta(D/2 - r_\theta)\Theta(-\omega)], \qquad (27)$$

where the normalization factor

$$A = Q^*\{4\pi R[1 + \cos\theta_0(1 - \ln\cos\theta_0)]\}^{-1} \qquad (28)$$

guarantees that $\int_{V_{in}} d^3r\varrho_{in}(\mathbf{r}) = Q^*$.

We rewrite Eq. (8), expressing $U_H(D)$ by using the electrostatic potential $\Phi(\mathbf{r})$ as

$$U_H(D) = \frac{1}{2\epsilon}\left[\int_{V_{in}} d^3r(\Phi_{in}(\mathbf{r}) + \Phi_{out}(\mathbf{r}))\varrho_{in}(\mathbf{r})\right.$$

$$\left. + \int_{V_{out}} d^3r((\Phi_{in}(\mathbf{r}) + \Phi_{out}(\mathbf{r}))\varrho_{out}(\mathbf{r})\right], \qquad (29)$$

where $\Phi_\alpha(\mathbf{r})$ ($\alpha = $ in, out), is the contribution of the charge density $\varrho_\alpha(\mathbf{r})$ to the electrostatic potential at an *arbitrary* point $\mathbf{r}$ in space. The calculation of $\Phi_{in}(\mathbf{r})$ is rather technical and is shown in Appendix A; that of $\Phi_{out}(\mathbf{r})$ in Appendix B. Unlike the single-star cases, an analytical solution is no longer feasible and therefore numerical computations are necessary in order to determine the electrostatic energy. On dimensional grounds, $U_H(D)$ has the form

$$\frac{U_H(D)}{k_BT} = \frac{Z^2\lambda_B}{R} h\left(\frac{R_W}{R}, \frac{D}{R}\right)$$

$$= \frac{Z^2\lambda_B}{R}\left[h_{in\text{-}in}\left(\frac{D}{R}\right) + 2h_{in\text{-}out}\left(\frac{R_W}{R}, \frac{D}{R}\right)\right.$$

$$\left. + h_{out\text{-}out}\left(\frac{R_W}{R}, \frac{D}{R}\right)\right], \qquad (30)$$

where $Z = Q^*/|e|$ is the *total* number of uncompensated charges of *both* spheres and $h_{\alpha-\beta}(R_W/R, D/R)$ ($\alpha, \beta = $ in, out) are dimensionless functions arising from the integrations
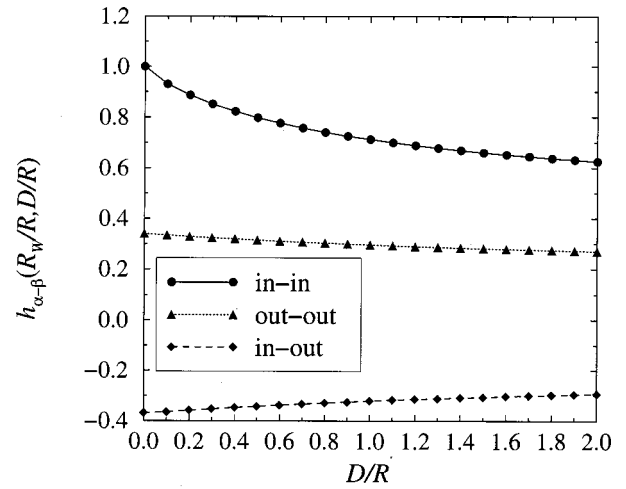

FIG. 7. The three terms contributing to the electrostatic energy of two PE stars, according to Eq. (30), as functions of the center-to-center separation D for $R_W = 1.65R$.

of the products $\Phi_\alpha(\mathbf{r})\varrho_\beta(\mathbf{r})$ in Eq. (29). Note that the first term, $h_{in\text{-}in}$, has *no* R_W dependence. The various contributions of the terms at $R_W = 1.65R$ are shown in Fig. 7. The strongest D dependence arises from the integration of the term $\Phi_{in}(\mathbf{r})\varrho_{in}(\mathbf{r})$. The other terms are weaker, both in their energy scale and in their D dependence.

We proceed with the calculation of the entropic terms $S_i(D)$, $(i=1,2,3)$, which include the D-dependent volumes of integration and their corresponding profiles $\rho_i(\mathbf{r})$. In particular, $\rho_1(\mathbf{r})$ is uniform within the $2f$ tubes and zero otherwise. The trapped counterion density $\rho_2(\mathbf{r})$ has the form $\rho_2(\mathbf{r}) = B[P(\mathbf{r}) + P(\mathbf{D} - \mathbf{r})]$, with the shape function $P(\mathbf{r})$ given by Eq. (27). The constant B is determined by the condition $\int_{V_2} d^3r\rho_2(\mathbf{r}) = N_2$, where $V_2(D) = V_{in}(D) - V_1$ (here $V_1 = 2f\pi\lambda_B^2 R$), and reads as
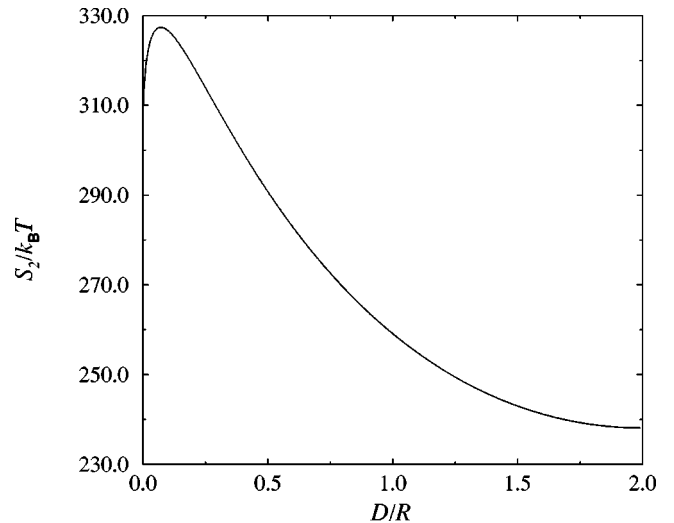

FIG. 8. Entropic contribution of trapped counterions (here $N_2 = 100$) vs star–star separation D.

$$B = \frac{N_2}{4\pi R\left[\frac{D}{2R}\left(1 - \ln\left(\frac{D}{2R}\right)\right) + 1\right]}. \quad (31)$$

Finally, $\rho_3(\mathbf{r}) = N_3/V_{\text{out}}(D)$. Accordingly, we obtain the entropic contributions of the counterions in the three different states using Eq. (12) as

$$\frac{S_1}{k_B T} = N_1\left[\ln\left(\frac{N_1 \sigma_{\text{LJ}}^3}{\widetilde{V}_1}\right) - 1\right]; \quad (32)$$

$$\frac{S_2}{k_B T} = N_2 \ln\left(\frac{N_2}{4\pi\left[1 + \frac{D}{2R'}\left(1 - \ln\left(\frac{D}{2R'}\right)\right)\right]}\right)$$

$$+ \frac{N_2}{1 + \frac{D}{2R'}\left(1 - \ln\left(\frac{D}{2R'}\right)\right)}\frac{D}{2R'}\ln^2\left(\frac{D}{2R'}\right)$$

$$+ N_2 + 3N_2 \ln\left(\frac{R}{R'}\right); \quad (33)$$

$$\frac{S_3}{k_B T} = N_3\left[\ln\left(\frac{N_3}{4\pi\left[\frac{1}{3}\left(\frac{R_W^3}{R^3} - 1\right) + \frac{D}{4R}\left(\frac{R_W^2}{R^2} - 1\right)\right]}\right) - 1\right], \quad (34)$$

where $\widetilde{V}_1 = V_1 - 2f\pi\sigma_{\text{LJ}}^2 R$. The last term of S_2 results from the fact that the available volume for the trapped counterions is reduced by the tubes around the chains. We therefore introduce two smaller fused spheres with radius $R' \leqslant R$ that fulfill the condition

$$V_{\text{in}}(R,D) - 2\pi f\lambda_B^2 R = V_{\text{in}}(R',D), \quad (35)$$

with

$$V_{\text{in}}(R',D) = \frac{4\pi}{3}R'^3\left[1 + \frac{3}{2}\left(\frac{D}{2R'}\right) - \frac{1}{2}\left(\frac{D}{2R'}\right)^3\right]. \quad (36)$$

R' is obtained by solving Eq. (35) together with Eq. (36) and it depends additionally on D.

We emphasize that the dominant D dependence of the two-star free energy [Eq. (25)] arises from the terms $U_H(D)$ and $S_2(D)$. The former is shown in Fig. 7 and the latter in Fig. 8. Three remarks are in order here: first, the number of trapped counterions $N_2 = N_{\text{in}} - N_1$ sets the overall scale of the term $S_2(D)$. Therefore the role of the N_1 condensed counterions becomes important in "renormalizing" the effec-

tive interaction, as we will explain shortly. Second, both $U_H(D)$ and $S_2(D)$ are nonlinear functions of D, implying that the resulting effective force $F(D) = -dV_{\text{eff}}(D)/dD$ is is *not* constant. This finding is at odds with the the the situation in curved polyelectrolyte brushes, resulting from grafting PE chains on a solid particle of radius b. By employing scaling arguments for the trapped counterions, Pincus predicted that in the regime $R \gg D \gg b$ the force of two porcupines is D independent.[19] Finally, we comment on the fact that $S_2(D)$ in Fig. 8 shows a maximum for a small but nonzero value of the separation, $D \cong 0.1R$. This is an artifact of the model for the density distributions, in which we assumed a $\sim r^{-2}$ dependence of the profiles for all r. In reality, the monomer and counterion densities do not diverge at $r = 0$ due to the hard cores of the particles. Hence, at small separations, strong steric repulsions between the locally dense macromolecular aggregates will cause the entropy $S_2(D)$ to increase monotonically as $D \to 0$. Neither in the simulations nor in the theory, however, did we examine the effective interaction at such small separations, hence this artifact does not influence the comparisons that are to follow.

The effective potential $V_{\text{eff}}(D)$ is obtained by adding up the terms $S_i(D)$ and $U_H(D)$, according to Eq. (25) and *minimizing* the free energy $\mathcal{F}_2(D;R,\{N_i\})$ with respect to R and the N_is for every separation $D \leqslant 2R$. We can simplify the problem by first taking into consideration that the star extent R is unaffected by D. Indeed, the chains are already almost completely stretched and, as confirmed during our simulation runs, R remains constant and equal to its value for the isolated star. Since the N_is are related through $N_1 + N_2 + N_3 = N_c = \text{constant}$, only two variational parameters remain, say N_1 and N_2. In the simulations we have found that the number of condensed counterions remains, to a very good approximation, constant for all overlapping separations $D \leqslant 2R$, and undergoes a rather abrupt change at the crossover distance $D = 2R$. Hence, we have chosen *not* to determine N_1 through the variational calculation, but rather to treat it as a fit parameter, held constant for all D, and chosen so as to give optimal agreement with simulation results. It would be desirable to obtain this result through the full minimization; however such an attempt leads to significantly worse results than the procedure described above. On the other hand, the treatment of the net charge as a fit parameter is not at all unusual for charged systems and, in the realm of charge-stabilized colloidal suspensions, it is an oft-used approach known as *charge renormalization*.[42,44,45] Therefore, $\mathcal{F}_2(D,;R,\{N_i\})$ is only minimized with respect to N_2, yielding

$$N_2(D) = \frac{R}{2\lambda_B h\left(\frac{R_W}{R},\frac{D}{R}\right)}\left\{2 + \frac{D}{2R'}\frac{\ln^2\left(\frac{D}{2R'}\right)}{1 + \frac{D}{2R'}\left(1 - \ln\left(\frac{D}{2R'}\right)\right)} + \ln\left[\left(\frac{N_c - N_1}{N_2} - 1\right)\frac{\frac{1}{3}\left(\frac{R_W^3}{R^3} - 1\right) + \frac{D}{4R}\left(\frac{R_W^2}{R^2} - 1\right)}{1 + \frac{D}{2R'}\left(1 - \ln\left(\frac{D}{2R'}\right)\right)}\left(\frac{R}{R'}\right)^3\right]\right\}, \quad (37)$$

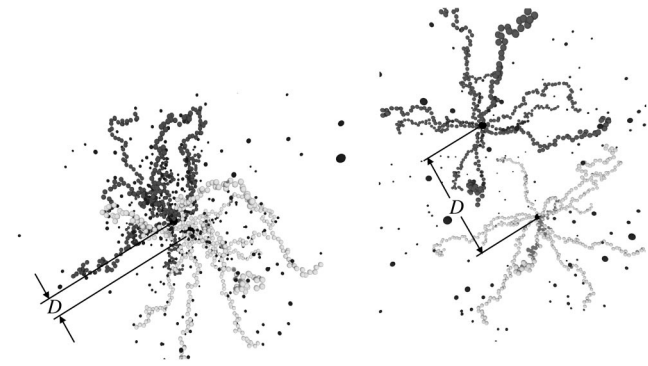with R' obtained by solving Eq. (36).

FIG. 9. Simulation snapshots of two polyelectrolyte-stars at small center-to-center separation D (left picture) and at a larger separation (right picture). The chain length is $N = 50$ and the arm number $f = 10$.

TABLE IV. The parameters used in the simulations of two PE stars. The degree of polymerization is $N = 50$ for all entries. R_d is the core size, scaled on the radius R obtained from Table I. In the last two columns, we show in addition the parameter values for the force fit of Eq. (39).

f	α	N_c	(R_d/R)	N_1	ζ	$\tilde{C}$
5	1/3	80	0.01	105	0.47	0.0542
10	1/6	80	0.05	80	0.43	0.0456
10	1/4	120	0.05	147	0.45	0.0343
10	1/3	160	0.04	218	0.52	0.0265
18	1/6	144	0.06	160	0.50	0.0238
18	1/4	216	0.05	275	0.56	0.0183
18	1/3	288	0.05	400	0.59	0.0149
30	1/4	360	0.08	265	0.63	0.0114

B. Results for the effective interaction

The theoretical model for the effective interaction has been tested against results of MD simulations of two star-branched polyelectrolytes. In a MD simulation, the mean force at the center of the stars can be measured.[30,43] For this purpose, the simulation model of an isolated star, presented in Sec. II A, is expanded to two stars. The microscopic interaction potentials and parameters are those presented in Sec. II A. The centers of the two stars were placed along the body diagonal of the cubic simulation box with periodic boundary conditions and the mean force acting at the center of the stars was measured.[30] Typically 120 000 time steps are used for equilibration and up to 500 000 steps were simulated to gather statistics. For deep overlaps of the stars within their radii, the periodic images of the stars have negligible effects on the effective force. We have also checked that the image charges have only a minor effect on the measured forces at bare overlaps. In Fig. 9, snapshots of two PE stars at different separations D are shown, in order to illustrate the procedure and the typical conformation of the stars when they are close to one another. It is clear that there is no interdigitation from different stars.

Consider, then, two PE stars, $i = 1,2$, separated by a distance D. The mean force $\mathbf{F}_i(D)$ acting at the center of the ith star has two contributions, arising by the core-bonded monomers and all other nonbonded monomers acting on the core. Under these circumstances, the effective force $\mathbf{F}_i(D)$ acting on the ith star center is given as a canonical average

$$
\mathbf{F}_i(D) = \left\langle -\nabla_{\mathbf{R}_i}\left(\sum_{k=1}^{2\,fN} V_{\mathrm{LJ}}^c(|\mathbf{r}_k - \mathbf{R}_i|) \right. \right.
$$
$$
\left. \left. + \sum_{l=1}^{f} V_{\mathrm{FENE}}^c(|\mathbf{r}_l - \mathbf{R}_i|) \right) \right\rangle, \tag{38}
$$

where in the first sum the repulsive interactions of the core with *all* $2\,fN$ monomers in the system are considered according to Eq. (3), whereas the second sum only accounts for the attractive interactions with the f innermost monomers of the chains attached to the ith center according to Eq. (4). In what follows, we consider the projection $F(D) = \mathbf{F}_1(D) \cdot (\mathbf{R}_1 - \mathbf{R}_2)/|\mathbf{R}_1 - \mathbf{R}_2|$ of the effective force on the interparticle axis, related to the effective interaction through[43] $F(D) = -dV_{\mathrm{eff}}(D)/dD$.
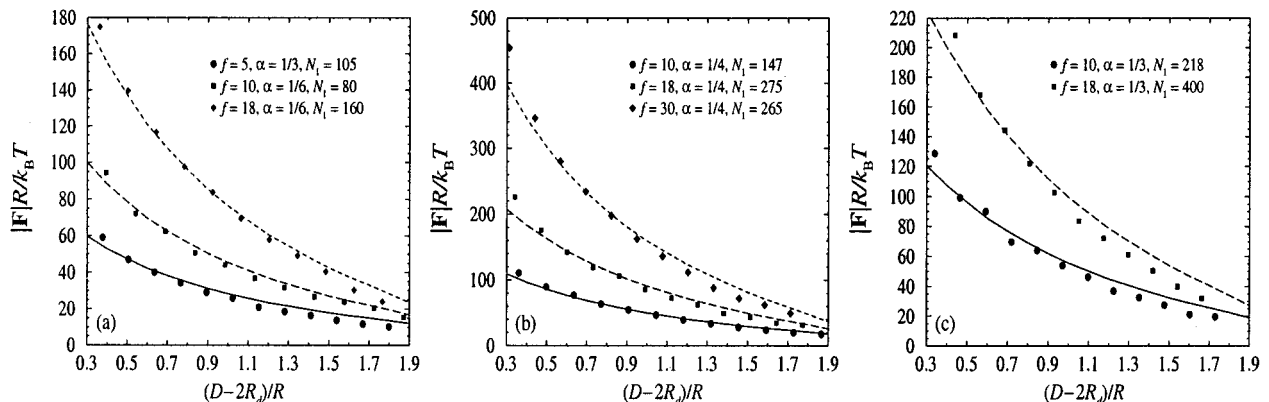

FIG. 10. Theoretical results (lines) in comparison with simulation results (symbols) of the effective forces $F(D)$ for different parameter combinations f, α, and N_1. The chain length is fixed at $N = 50$. Since the theoretical model has no core, in contrast to the simulation model, the simulation data have to be displaced by the core diameter $2R_d$. [(a) and (b) redrawn from Ref. 26].

The parameter combinations for which we performed simulations are summarized in Table IV. The results, compared with the theoretical predictions of Sec. III A, are shown in Fig. 10. As can be seen, there is very good agreement between theory and simulation, for all parameter combinations considered. The number of condensed counterions N_1 lies for all curves between twice the value calculated for a star with f arms and the value for a star with $2f$ arms, which formally is obtained at zero separation between the two macromolecules. The only exception is the case with $f = 5$; however, for such a low arm number the assumption of chain retraction and the associated cut of the density profile at the bisecting plane are probably not valid. Nevertheless, good agreement with the simulation results is obtained with the choice $N_1 = 105$. The *shape* of the force is determined almost entirely by the entropic term S_2 and the electrostatic contribution U_H plays only a minor role, as the PE stars are almost electroneutral. This is in full agreement with the predictions of Ref. 19. The *magnitude* of the force is determined mainly by the amount of mobile counterions $N_2 = N_{in} - N_1$ inside, hence the amount of condensed counterions plays a decisive role. Moreover, a homogeneous charge and density distribution inside the star leads to the erroneous prediction that the force is almost constant, hence the $\sim 1/r^2$ profiles are crucial in reproducing the shape of the force versus distance curves.

In order to cast the effective interaction into a manageable form that should facilitate the theoretical analysis of experimental scattering data, we derive a simple and accurate fit of the force data, which is shown in Fig. 11. The fit is given by

$$2R\frac{F(D)}{k_B T} = C(f,N_c)\left[\left(\frac{D}{2R}\right)^{-\zeta} - 0.4\left(\frac{D}{2R}\right)^{1-\zeta}\right], \quad (39)$$

with $0.4 \lesssim \zeta \lesssim 0.63$, and a positive constant C. For the latter, we further introduce the ansatz

$$C(f,N_c) = \tilde{C}fN_c. \quad (40)$$

The precise values for ζ and $\tilde{C}$ depend on f and N_c (or α) and are listed in the last two columns of Table IV. The exponent ζ always remains smaller than the value $\zeta_{neutral} = 1$, which is obtained for neutral star polymers[30,46] ($F \sim D^{-1}$). For neutral stars, a weakly diverging logarithmic effective interaction results,[46,47] whereas in this case the effective interaction does not diverge at the origin.

Further, the interaction beyond overlap must be determined. For this purpose, we assume that the charged monomers of one star interact with the charged monomers of the other star via a screened potential of the Yukawa form, the screening caused by the counterions surrounding the stars. Integrating these Yukawa segments on both stars leads to a Yukawa-type tail for the effective interaction between stars at large separations as well. This is in line with the theory of effective interactions for charged colloids[42] as well as with recent results from linear-response theory applied to polyelectrolyte-stars.[48] Matching the expression valid for $D \leq 2R$, Eq. (39), with the expression
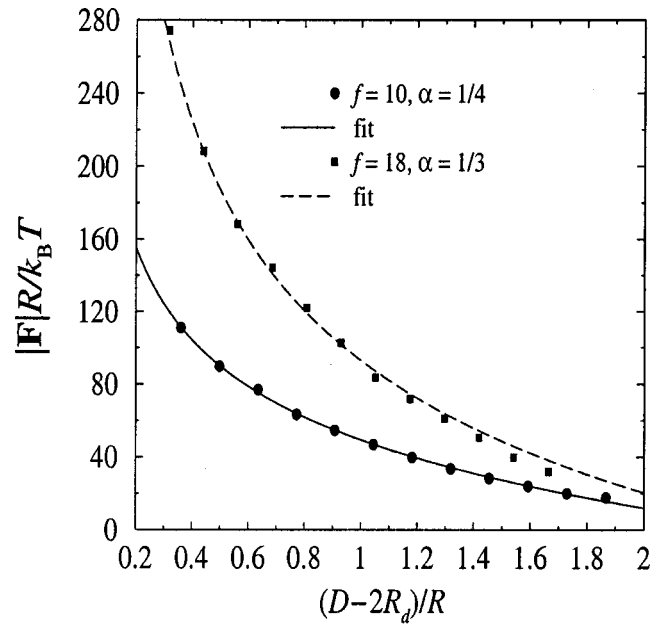

FIG. 11. Fit (lines) of the simulation data (symbols) for the effective force between two PE stars, according to Eq. (39).

$$F(D) \propto -\frac{d}{dD}\frac{\exp(-\kappa D)}{D}, \quad (41)$$

valid for $D > 2R$, leads to

$$2R\frac{F(D)}{k_B T} = \tilde{C}fN_c \begin{cases} \left(\dfrac{D}{2R}\right)^{-\zeta} - \dfrac{2}{5}\left(\dfrac{D}{2R}\right)^{1-\zeta} & \text{for } D \leq 2R; \\ \dfrac{3}{5}(1+2\kappa R)^{-1}(1+\kappa D)\left(\dfrac{2R}{D}\right)^2 \\ \quad \times \exp[-\kappa(D-2R)] & \text{for } D \geq 2R, \end{cases} \quad (42)$$

where $\kappa = \sqrt{\rho_3 \lambda_B}$ is the inverse Debye screening length. Therefore, the interaction potential $V_{eff}(D)$, obtained by integration of Eq. (42), reads as

$$\frac{V_{eff}(D)}{k_B T}$$

$$= \tilde{C}fN_c \begin{cases} \dfrac{1}{1-\zeta}\left[1-\left(\dfrac{D}{2R}\right)^{1-\zeta}\right] + \dfrac{2}{5(2-\zeta)}\left[\left(\dfrac{D}{2R}\right)^{2-\zeta}-1\right] \\ \quad + \dfrac{3}{5}(1+2\kappa R)^{-1} \quad \text{for } D \leq 2R; \\ \dfrac{3}{5}(1+2\kappa R)^{-1}\left(\dfrac{2R}{D}\right)\exp[-\kappa(D-2R)] \\ \quad \text{for } D \geq 2R. \end{cases} \quad (43)$$

The last expression can be used in attempting to describe theoretically scattering profiles from concentrated PE star solutions.[20,23,49] The effective interaction is manifestly density dependent through the inverse Debye length κ. For the
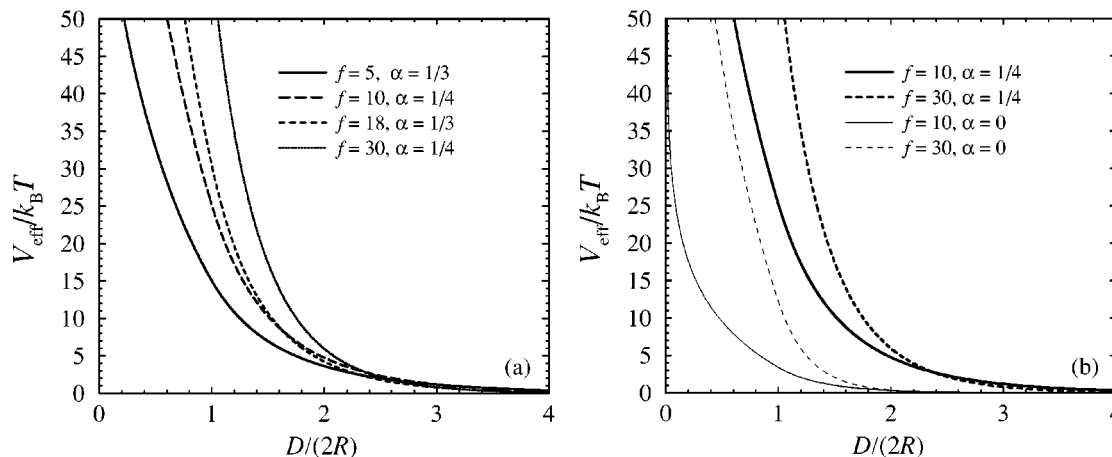
FIG. 12. (a) The effective interaction potential $V_{\rm eff}(D)$ obtained from Eq. (43) for various f and α values. (b) A comparison between the effective interactions between charged stars (thick lines) and those for neutral stars [thin lines, obtained from Eq. (44)], having the same arm number and size as the charged ones.

purpose of fitting experimental data, $\widetilde{C}$ and ζ can be used as fit parameters, however the constraint $0<\zeta<1$ should always be respected.

Representative curves for the effective interaction of Eq. (43) are shown in Fig. 12(a). As can be seen from Eq. (43), the potential between polyelectrolyte stars has the property of being *bounded*, i.e., its value at zero separation between the stars is finite. This is an idealization stemming from the fact that we assumed, in the theoretical modeling, that the central particle on which the chains are anchored has vanishing extent. Although in reality the effective interaction will diverge at full overlaps, the range of this divergence will be very small, typically on the order of a few Å. On the other hand, the range of the interaction derived above is that of the corona radius of the stars, which can be very large, up to several microns for long chains. Hence, for a vast range of star concentrations, the macromolecules will feel only the effects of the ultrasoft interaction of Eq. (43) and a theoretical analysis on the basis of the latter will be fully sufficient in capturing the physics of the correlations in the system. In this respect, the effective interaction between PE stars belongs to a new class of potentials that have attracted considerable attention recently, the so-called mean-field potentials.[43,50–58] Physical systems whose constituent particles interact by means of such a bounded or a slowly diverging interaction, are called mean-field fluids.[43,55,58] Typical phenomena associated with mean-field fluids are an anomalous structure factor in the fluid phase,[50,59] reentrant melting and exotic crystal structures in the solid phase,[50,60–62] as well as the property that at high concentrations in the uniform phase the direct correlation function of the system is, to an excellent approximation, equal to $-V_{\rm eff}(r)/(k_BT)$.[50–55] Polymer chains,[52,53] dendrimers,[54] as well as neutral star polymers[58] are systems that have been shown to belong to this new class. Polyelectrolyte stars are the new member of the family.

It is pertinent to compare the effective interaction of Eq. (43), valid for *charged* star polymers, with the known interaction for *neutral* stars.[47] The latter features an ultrasoft, logarithmic divergence for overlapping stars and a Yukawa

decay for nonoverlapping ones, hence it has some qualitative similarities with the interaction of PE stars, and reads as[47]

$$\frac{V_{\rm eff}(D)}{k_BT}$$

$$= \frac{5}{18}f^{3/2}\begin{cases} -\ln\left(\dfrac{D}{2R}\right)+(1+\sqrt{f}/2)^{-1} & \text{for } D\leqslant 2R; \\[2ex] (1+\sqrt{f}/2)^{-1}\left(\dfrac{2R}{D}\right)\exp\left[-\dfrac{\sqrt{f}(D-2R)}{4R}\right] \\[1ex] \quad \text{for } D\geqslant 2R. \end{cases}$$

(44)

The comparison is shown in Fig. 12(b). Despite the fact that the potential of Eq. (44) diverges at the origin and that of Eq. (43) does not, the latter represents nevertheless much stronger repulsions at strongly overlapping configurations than the former. Although the interaction between neutral stars formally takes over at some small separation D, due to its divergence, the ultrasoft character of the latter renders this crossover value very small. Hence, polyelectrolyte stars repel each other at overlapping separations much more strongly than their neutral counterparts. This implies that stabilization of colloidal particles against the van der Waals attraction can be achieved more efficiently by grafting of polyelectrolytes than by grafting of neutral polymer chains.

C. Interacting stars in the presence of added salt

In this section we turn our attention to the effective interaction in the presence of added salt. As discussed in Sec. II D, the coions of the added salt remain outside the star, whereas in the salt-free case only a very small fraction of counterions can be found there. In addition, the salt counterions just supplement a small fraction to neutralize the star, hence they are also predominantly found in the star exterior. Therefore, we obtain in the case of added salt a drastically increased entropic contribution S_3 from the outside region, in comparison to the salt-free case. The available volume $V_{\rm out}$ to the counter- and coions outside the star and its dependence
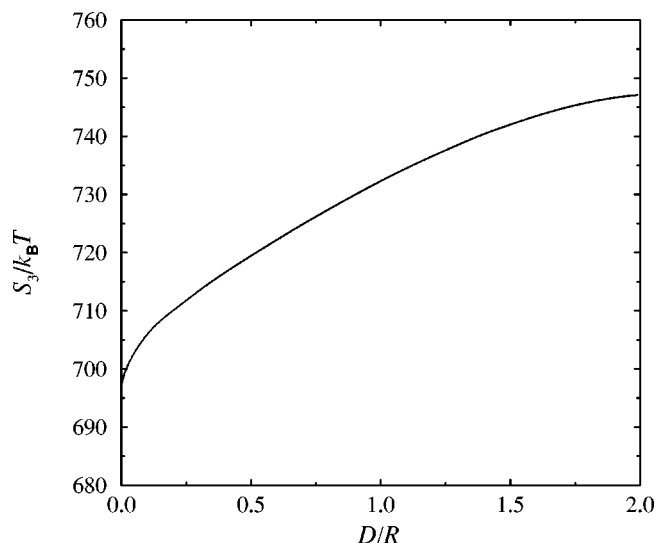
FIG. 13. The D dependence of the entropic contribution of the counterions and the coions outside the stars for the case of added salt. The parameters are $f=10$, $\alpha=1/3$, $N_c=320$, with $N_s=250$ added salt molecules. The Wigner–Seitz radius is $R_W=55.83\sigma_{\mathrm{LJ}}$.
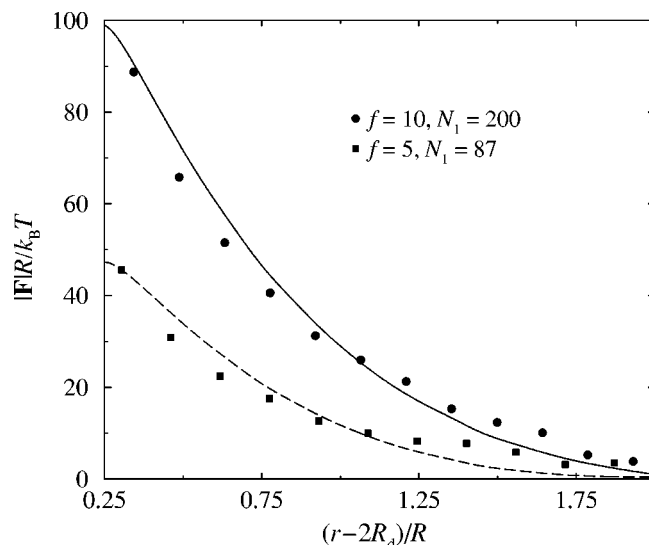

FIG. 14. Theoretical (lines) and simulation (points) results for the force between two stars in the presence of added salt. The degree of polymerization of the chains is $N=50$, the charging fraction $\alpha=1/3$ and for $N_s=250$ salt molecules in the simulation box, corresponding to a salt concentration $c_s=0.036$ M.

on the star–star separation D now plays an important role in diminishing the magnitude of the effective force between the PE stars. Indeed, V_{out} increases with decreasing distances between the stars D. As the volume available to the counter- and coions increases with decreasing D, their entropy also grows. The dependence of the term $S_3(D)$ on D is shown in Fig. 13.

Since we have a large number of particles in the outside region, this entropy increase is significant and contributes a measurable effective attraction to the total potential between the stars. Alternatively, one can think of the two overlapping stars in Fig. 6 as being hit by a large number of counterions mostly from the outside, a situation that results an unbalanced force pushing the two stars closer to one another. This is the well known "depletion mechanism,"[43] familiar from the classical case of colloid–polymer mixtures,[63] in which the small polymer induces an attraction between the large, hard colloids. An important quantitative difference in the case at hand, though, is that the large stars are *not* hard but penetrable. Thus, the depletion attraction is superimposed on the repulsion caused by the trapped counterions and the total effect need not be a net attraction. Instead, a reduced repulsion between the polyelectrolyte stars results.

The theoretical analysis of the effective interaction in the case of added salt follows the same lines presented in Sec. III A above. Similarly to the single-star case, we have to make the formal substitution $N_3=N_c-N_{\mathrm{in}}\rightarrow N_c+2N_s-N_{\mathrm{in}}$, when N_s salt molecules are present. Now the D dependence of the volume $V_{\mathrm{out}}(D)$ becomes crucial in comparison with simulation results, since the size L_b of the simulation box remains constant and $V_{\mathrm{out}}(D)$ grows as D diminishes. Referring to Fig. 6, we see that the D-dependent Wigner–Seitz radius $R_W(D)$ can be determined by solving the equation

$$L_b^3=V_{\mathrm{out}}(D)+V_{\mathrm{in}}(D). \tag{45}$$

The expression for the Wigner–Seitz radius reads as

$$R_W(D)=\begin{cases} \left(\dfrac{3}{4\pi}\right)^{1/3}L_b & \text{for } D=0; \\[2ex] \dfrac{D}{2}\left[\cosh\left(\dfrac{\psi}{3}\right)-\dfrac{1}{2}\right] & \text{for } D>0, \end{cases} \tag{46}$$

where ψ is given by

$$\psi=\ln[w+\sqrt{w^2-1}], \tag{47}$$

with

$$w=1+\frac{24}{\pi}\left(\frac{L_b}{D}\right)^3. \tag{48}$$

The theoretical results obtained with these modifications are shown in Fig. 14, and compared with simulations. Both data sets correspond to a salt concentration of $c_s=0.036$ mol/l. It can be seen indeed that the magnitude of the force is roughly halved in comparison with the salt-free cases of Fig. 10. The osmotic pressure from the outer ions has the effect of reducing the strength of the star–star interaction for overlapping stars. For nonoverlapping stars, the same effect appears, for the well-understood reason of enhanced screening, causing an increase of the inverse Debye screening length κ in Eq. (43).

IV. SUMMARY AND CONCLUDING REMARKS

We have analyzed the conformations, sizes, counterion distributions and effective interactions between osmotic polyelectrolyte-stars. The main findings of this work are: (i) a stretching of the arms of the stars; (ii) a strong absorption of counterions in the star interior and condensation along the rodlike chains; (iii) an entropically dominated, soft effective

repulsion between PE stars, being caused mainly by the trapped counterions; and (iv) a reduction of the strength of the repulsion in the presence of added salt.

The crossover of the effective interaction from a power-law form at overlaps to a Yukawa form beyond overlaps is akin to the case of neutral star polymers. Hence, it is to be expected that the anomalous structure factors found there[59] will also be seen in the case of charged stars if the concentration of the solution exceeds its overlap value. On similar grounds, an unusual phase diagram for PE stars is also to be expected,[60] displaying exotic crystals and reentrant melting. The phase diagram will be much richer in this case, due to the addition of two more possible degrees of freedom: the charging fraction α and the salt concentration. Additional questions that should be addressed in future investigations include the effects of polydispersity[64] and many-body forces[65] in polyelectrolyte-star solutions. The latter are expected to play a minor role at reasonable concentrations, though, because the entropy argument suggests they will become important only at densities for which three PE stars have a triplet overlap within their coronae, and higher. Finally, further work should be done to study spherical PE brushes[20,66] having a nonvanishing hard colloidal particle in the middle of the aggregate and a corresponding core–shell structure.

ACKNOWLEDGMENTS

APPENDIX A: CALCULATION OF THE ELECTROSTATIC POTENTIAL Φ_{in}

In this Appendix we present the technical details for the calculation of the electrostatic potential of the two fused spheres of radius R, each carrying a charge Q^* and having a charge density $\varrho(\mathbf{r}')$ that decays as $(r')^{-2}$ with the distance r' from its center and is abruptly cut off at the mid plane, as given by Eqs. (26) and (28). In other words, we show the steps for the calculation of the electrostatic potential $\Phi_{in}(\mathbf{r})$ of Eq. (29).

The electrostatic potential $\Phi(\mathbf{r})$ due to the charge density $\varrho(\mathbf{r})$ in a dielectric medium of permittivity ϵ is given by

$$\Phi(\mathbf{r}) = \frac{1}{\epsilon} \int \frac{\varrho(\mathbf{r}')}{|\mathbf{r}' - \mathbf{r}|} d^3 r'. \tag{A1}$$

In order to calculate the integral above, we now take the two inner fused spheres shown in Fig. 6 and introduce infinitesimally thin disks of thickness dz' that are perpendicular to the z axis and cover the whole pattern, as shown in Fig. 15. There, we show for clarity only one of the two fused spheres, cut in the mid plane, which we call a "chopped sphere" and which can be figured as a succession of disks, each carrying an elementary charge dQ. It is a straightforward calculation to show that this elementary charge is given by
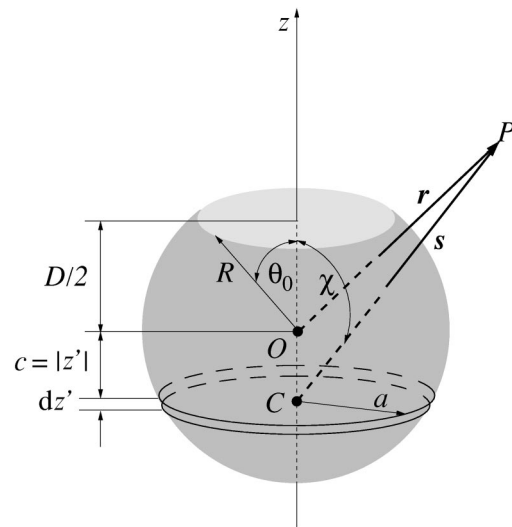

FIG. 15. A sketch of the chopped sphere showing the geometry of the problem and demonstrating the procedure used for the calculation of the electrostatic potentials.

$$dQ = \frac{Q^*}{2R} \ln\left(\frac{R}{c}\right) \frac{1}{1 + \cos\theta_0 [1 - \ln(\cos\theta_0)]} dz', \tag{A2}$$

i.e., it depends on the geometry through $\cos\theta_0 = D/(2R)$ as well as on the position of the disk center C along the z axis. As shown in Fig. 15, c is the distance (OC) between the disk center and the center of the chopped sphere, which is taken to be the origin of the coordinate axes. With $C = (x', y', z')$ we have therefore

$$c = |z'|, \tag{A3}$$

whereas the radius a of the disk is given by

$$a = \sqrt{R^2 - z'^2}. \tag{A4}$$

The elementary contribution of the disk to the electrostatic potential at the point P, $d\Phi_{disc}(\mathbf{r}; z')$, depends parametrically on the disk center location z'. Its calculation follows from further decomposing the disk into concentric rings of radius ξ centered at C, making use of the known results for the electrostatic potential of a charged ring,[67,68] and integrating thereafter from $\xi = 0$ to $\xi = a$. Note that, due to the inhomogeneous $\propto (r')^{-2}$ dependence of the charge density inside the sphere, we are now dealing with disks that have inhomogeneous charge densities as function of ξ themselves, and which vary as $\propto (\xi^2 + c^2)^{-1}$. The integration over the rings can be nevertheless carried out analytically.

We employ cylindrical coordinates and also introduce the vector $\mathbf{s}$ connecting the disk center with the observation point P (see Fig. 15). We have, evidently, $\mathbf{r} = (\rho, \phi, z)$ and $\mathbf{s} = (\rho, \phi, z - z')$, with the distance from the z axis ρ and the azimuthal angle ϕ. Due to azimuthal symmetry, it holds $d\Phi_{disc}(\mathbf{r}; z') = d\Phi_{disc}(\rho, z; z')$. It is convenient as an intermediate step to express the sought-for potential in a shifted system of axes, whose origin lies at the center C of the disk, and in which the potential is expressed by another function $d\Phi'$, i.e., we write
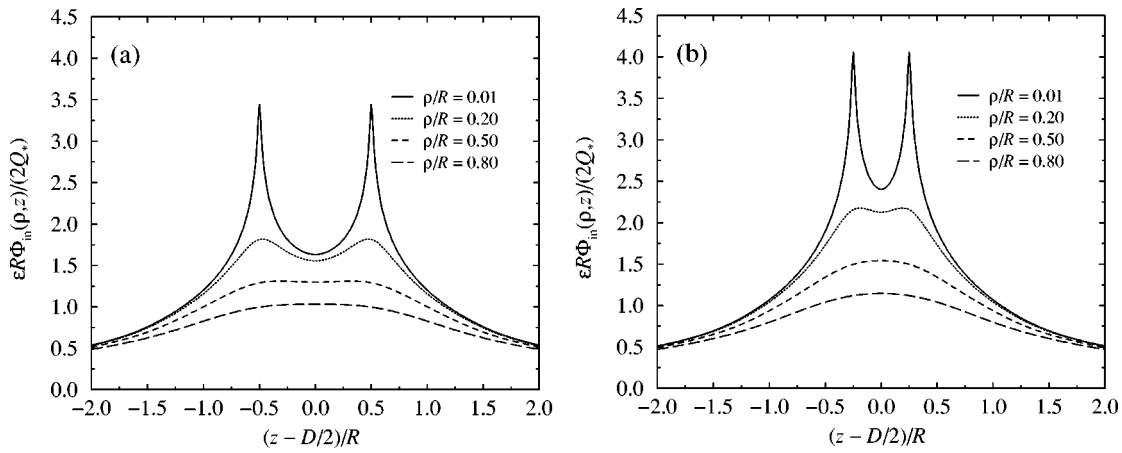
FIG. 16. The electrostatic potential $\Phi_{in}(\mathbf{r})$ for two inhomogeneously charged, chopped fused spheres of radius R, plotted as a function of z along paths of fixed distance ρ from the z axis. (a) Center-to-center distance $D=R$; (b) $D=R/2$. The curves are shown in the cylindrical coordinates introduced in Fig. 15. The centers of the spheres are located at the z positions for which the upper curves have sharp peaks.

$$d\Phi_{disc}(\rho,z;z') = d\Phi'(\rho,z-z';z')$$

$$= d\Psi(s,\chi;z'). \tag{A5}$$

Here, s is the magnitude of the vector $\mathbf{s}$ and χ is the angle between $\mathbf{s}$ and the z axis. The coordinates s and χ are related to the original ones through

$$s = \sqrt{\rho^2 + (z-z')^2}; \tag{A6}$$

$$\cos\chi = \frac{z-z'}{\rho^2 + (z-z')^2}. \tag{A7}$$

The function $d\Psi(s,\chi;z')$ can be obtained analytically through the integration over rings mentioned above. The result reads as follows:

$$d\Psi(s,\chi;z') = \begin{cases} d\Psi_<(s,\chi;z') & \text{for } s \leq a; \\ d\Psi_>(s,\chi;z') & \text{for } s > a. \end{cases} \tag{A8}$$

The term $d\Psi_<(s,\chi;z')$ is given by

$$d\Psi_<(s,\chi;z')$$

$$= \frac{2dQ}{\epsilon \ln[1+(a/c)^2]} \frac{1}{c} \sum_{k=0}^{\infty} P_{2k}(0) P_{2k}(\cos\chi)$$

$$\times [A_k(s;z') + B_k(s;z')], \tag{A9}$$

where $P_m(x)$ is the Legendre polynomial of order m

$$A_k(s;z') = \left(\frac{s}{c}\right)^{-(2k+1)} \left\{ \frac{(-1)^k}{2} \ln\left[1 + \left(\frac{s}{c}\right)^2\right] \right.$$

$$\left. + \sum_{j=1}^{k} \frac{(-1)^{j+k}}{2j} \left(\frac{s}{c}\right)^{2j} \right\}, \tag{A10}$$

and

$$B_k(s;z') = \left(\frac{s}{c}\right)^{2k} \left\{ (-1)^k \left[\tan^{-1}\left(\frac{a}{c}\right) - \tan^{-1}\left(\frac{s}{c}\right) \right] \right.$$

$$\left. - \sum_{j=1}^{k} \frac{(-1)^{j+k}}{2j-1} \left[\left(\frac{c}{a}\right)^{2j-1} - \left(\frac{c}{s}\right)^{2j-1} \right] \right\}. \tag{A11}$$

The term $d\Psi_>(z,\mathbf{s})$ is given by

$$d\Psi_>(s,\chi;z')$$

$$= \frac{2dQ}{\epsilon \ln[1+(a/c)^2]} \frac{1}{c} \sum_{k=0}^{\infty} P_{2k}(0) P_{2k}(\cos\chi) \left(\frac{c}{s}\right)^{2k+1}$$

$$\times \left\{ \sum_{j=1}^{k} \frac{(-1)^{j+k}}{2j} \left(\frac{a}{c}\right)^{2j} + \frac{(-1)^k}{2} \ln\left[1 + \left(\frac{a}{c}\right)^2\right] \right\}. \tag{A12}$$

The electrostatic potential caused by the *single* chopped sphere $\Phi_{chop}(\mathbf{r})$ at point P can be obtained by a z' integration

$$\Phi_{chop}(\mathbf{r}) = \int_{z'=-R}^{z'=D/2} d\Phi_{disc}(\rho,z;z')$$

$$= \int_{z'=-R}^{z'=D/2} d\Psi(s(\rho,z;z'),\chi(\rho,z;z');z'). \tag{A13}$$

Due to symmetry, the *total* electrostatic potential $\Phi_{in}(\mathbf{r})$ caused by *both* fused spheres at the observation point P is given as

$$\Phi_{in}(\mathbf{r}) = \Phi_{chop}(\mathbf{r}) + \Phi_{chop}(\mathbf{D}-\mathbf{r}), \tag{A14}$$

where $\mathbf{D} = D\hat{\mathbf{e}}_z$. In Fig. 16, we show representative results for $\Phi_{in}(\mathbf{r})$ obtained with this procedure.

The integral in Eq. (A13) cannot be carried out analytically and one has to resort to a simple, one-dimensional numerical integration. In performing this integral by using Eqs. (A8)–(A12) together with Eqs. (A2)–(A7), all k and j sums appearing there must be made manifestly convergent, i.e., the sums have to be expressed in terms of a variable $x<1$ raised

to positive powers. For this purpose, it is necessary, depending on whether $s<c$ or $s>c$, to make expansions of the logarithmic and/or the inverse tangent functions in Eqs. (A10) and (A11). The expressions suitable for the numerical integration are given below for completeness and convenience.

Case I: $s<c<a$ or $s<a<c$.

$$d\Psi_<(s,\chi;z')$$

$$= \frac{2dQ}{\epsilon \ln[1+(a/c)^2]} \frac{1}{c} \sum_{k=0}^{\infty} P_{2k}(0)P_{2k}(\cos \chi)$$

$$\times [C_k(s;z')+D_k(s;z')+E_k(s;z')], \qquad (A15)$$

where

$$C_k(s;z') = \sum_{j=k+1}^{\infty} \frac{(-1)^{j+k+1}}{2j} \left(\frac{s}{c}\right)^{2(j-k)-1}; \qquad (A16)$$

$$D_k(s;z') = \left(\frac{s}{c}\right)^{2k} (-1)^k \left[\tan^{-1}\left(\frac{a}{c}\right) - \tan^{-1}\left(\frac{s}{c}\right)\right]; \qquad (A17)$$

$$E_k(s;z') = \sum_{j=1}^{k} \frac{(-1)^{j+k+1}}{2j-1} \left(\frac{s}{c}\right)^{2(k-j)+1} \left[\left(\frac{s}{a}\right)^{2j-1} - 1\right]. \qquad (A18)$$

Case II: $c<s<a$.

$$d\Psi_<(s,\chi;z')$$

$$= \frac{2dQ}{\epsilon \ln[1+(a/c)^2]} \frac{1}{c} \sum_{k=0}^{\infty} P_{2k}(0)P_{2k}(\cos \chi)[F_k(z,s)$$

$$+ G_k(z,s)+H_k(z,s)], \qquad (A19)$$

where

$$F_k(s;z') = \left(\frac{c}{s}\right)^{2k+1} \frac{(-1)^k}{2} \ln\left[1+\left(\frac{s}{c}\right)^2\right]; \qquad (A20)$$

$$G_k(s;z') = \sum_{j=1}^{k} \frac{(-1)^{j+k}}{2j} \left(\frac{c}{s}\right)^{2(k-j)+1}; \qquad (A21)$$

$$H_k(s;z') = \sum_{j=k+1}^{\infty} \frac{(-1)^{j+k}}{2j-1} \left(\frac{c}{s}\right)^{2(j-k)-1} \left[\left(\frac{s}{a}\right)^{2j-1} - 1\right]. \qquad (A22)$$

Case III: $a<s<c$.

$$d\Psi_>(s,\chi;z') = \frac{2dQ}{\epsilon \ln[1+(a/c)^2]} \frac{1}{c} \sum_{k=0}^{\infty} P_{2k}(0)P_{2k}(\cos \chi)$$

$$\times \sum_{j=k+1}^{\infty} \frac{(-1)^{j+k+1}}{2j} \left(\frac{a}{s}\right)^{2j} \left(\frac{s}{c}\right)^{2(j-k)-1}. \qquad (A23)$$

Case IV: $c<a<s$.

$$d\Psi_>(s,\chi;z') = \frac{2dQ}{\epsilon \ln[1+(a/c)^2]} \frac{1}{c} \sum_{k=0}^{\infty} P_{2k}(0)$$

$$\times P_{2k}(\cos \chi)[I_k(s;z')+J_k(s;z')], \qquad (A24)$$

where

$$I_k(s;z') = \sum_{j=1}^{k} \frac{(-1)^{j+k}}{2j} \left(\frac{a}{s}\right)^{2(k-j)+1} \left(\frac{c}{s}\right)^{2j}; \qquad (A25)$$

$$J_k(s;z') = \frac{(-1)^k}{2} \ln\left[1+\left(\frac{a}{c}\right)^2\right] \left(\frac{c}{s}\right)^{2k+1}. \qquad (A26)$$

Case V: $a<c<s$.

Here, $d\Psi_>(s,\chi;z')$ can be taken directly from Eq. (A12), as all parameters appearing in the sums are smaller than unity.

APPENDIX B: CALCULATION OF THE ELECTROSTATIC POTENTIAL Φ_{out}

In order to calculate the electrostatic potential $\Phi_{out}(\mathbf{r})$, caused by the hollow fused spheres of the free counterions that reside in the volume V_{out} (see Fig. 6), we employ the superposition principle. Thereby, the aforementioned hollow region of uniform charge density $\varrho_{out}(\mathbf{r})$ is apprehended as the superposition of two fused spheres of radius R_W with charge density $\varrho_{out}(\mathbf{r})$ and of two smaller fused spheres, of radius R, with charge density $-\varrho_{out}(\mathbf{r})$. In this way, the problem is reduced to the calculation of the electrostatic potential of two fused spheres with uniform charge density. The geometrical setup as well as the method of calculation are identical to those presented in Appendix A. Thereby, the electrostatic potential $d\Phi_{disc}(\mathbf{r})$ is still given by expressions of the form Eqs. (A5)–(A8), however Eqs. (A2), (A9), and (A12) have to be replaced by their counterparts valid for homogeneous charge distributions. The corresponding expressions for spheres of radius R are given below

$$dQ = \pi Q^*(R^2 - z'^2)$$

$$\times \left\{\frac{2\pi R^3}{3}\left[1+\frac{3}{2}\left(\frac{D}{2R}\right)-\frac{1}{2}\left(\frac{D}{2R}\right)^3\right]\right\}^{-1} dz', \qquad (B1)$$

$$d\Psi_<(s,\chi;z') = \frac{2dQ}{\epsilon a} \sum_{k=0}^{\infty} P_{2k}(0)P_{2k}(\cos \chi)$$

$$\times \left[\frac{4k+1}{2(k+1)(2k-1)} \left(\frac{s}{a}\right) - \frac{1}{2k-1} \left(\frac{s}{a}\right)^{2k}\right], \qquad (B2)$$

and

$$d\Psi_>(s,\chi;z') = \frac{2dQ}{\epsilon s} \sum_{k=0}^{\infty} \frac{P_{2k}(0)P_{2k}(\cos \chi)}{2(k+1)} \left(\frac{a}{s}\right)^{2k}. \qquad (B3)$$

The substitution $R \rightarrow R_W$ yields the expressions for the fused spheres of radius R_W. Note that the term in the curly brackets in Eq. (B1) is the volume of the chopped sphere.

[1] A. Yethiraj and C.-Y. Shew, Phys. Rev. Lett. **77**, 3937 (1996).
[2] A. Yethiraj, Phys. Rev. Lett. **78**, 3789 (1997).
[3] H. Schiessel and P. Pincus, Macromolecules **31**, 7953 (1998).
[4] N. V. Brillantov, D. V. Kuznetzov, and R. Klein, Phys. Rev. Lett. **81**, 1433 (1998).
[5] R. G. Winkler, M. Gold, and P. Reineker, Phys. Rev. Lett. **80**, 3731 (1998).
[6] J. Jiang, H. Liu, Y. Hu, and J. M. Prausnitz, J. Chem. Phys. **108**, 780 (1998).

[7] R. M. Nyquist, B.-Y. Ha, and A. Liu, Macromolecules **32**, 3481 (1999).

[8] Y. Kantor and M. Kardar, Phys. Rev. Lett. **83**, 745 (1999).

[9] R. Golestanian, M. Kardar, and T. B. Liverpool, Phys. Rev. Lett. **82**, 4456 (1999).

[10] L. Harnau and P. Reineker, J. Chem. Phys. **112**, 437 (2000).

[11] V. V. Vasilevskaya, A. R. Khokhlov, and K. Yoshikawa, Macromol. Theory Simul. **9**, 600 (2000).

[12] J. W. Jiang, L. Blum, O. Bernard, and J. M. Prausnitz, Mol. Phys. **99**, 1121 (2001).

[13] J.-F. Joanny, Eur. Phys. J. E **5**, 3 (2001).

[14] F. Vongoeller and M. Muthukumar, Macromolecules **28**, 6608 (1995).

[15] R. Hariharan, C. Biver, J. Mays, and W. B. Russel, Macromolecules **31**, 7506 (1998).

[16] E. B. Zhulina, J. Klein Wolterink, and O. V. Borisov, Macromolecules **33**, 4945 (2000).

[17] F. S. Csajka and C. Seidel, Macromolecules **33**, 2728 (2000).

[18] F. S. Csajka, R. R. Netz, C. Seidel, and J.-F. Joanny, Eur. Phys. J. E **4**, 505 (2001).

[19] P. Pincus, Macromolecules **24**, 2912 (1991).

[20] X. Guo and M. Ballauff, Langmuir **16**, 8719 (2000).

[21] J. Klein Wolterink, F. A. M. Leermakers, G. J. Fleer, L. K. Koopal, E. B. Zhulina, and O. V. Borisov, Macromolecules **32**, 2365 (1999).

[22] W. Groenenwegen, A. Lapp, S. U. Egelhaaf, and J. R. C. van der Maarel, Macromolecules **33**, 4080 (2000).

[23] W. Groenenwegen, S. U. Egelhaaf, A. Lapp, and J. R. C. van der Maarel, Macromolecules **33**, 3283 (2000).

[24] O. V. Borisov and E. B. Zhulina, Eur. Phys. J. B **4**, 205 (1998).

[25] O. V. Borisov and E. B. Zhulina, J. Phys. II **7**, 449 (1997).

[26] A. Jusufi, C. N. Likos, and H. Löwen, Phys. Rev. Lett. **88**, 018301 (2002).

[27] M. J. Stevens and K. Kremer, J. Chem. Phys. **103**, 1669 (1995).

[28] G. S. Grest, K. Kremer, and T. A. Witten, Macromolecules **20**, 1376 (1987).

[29] G. S. Grest, Macromolecules **27**, 3493 (1994).

[30] A. Jusufi, M. Watzlawek, and H. Löwen, Macromolecules **32**, 4470 (1999).

[31] W. Essafi, F. Lafuma, and C. E. Williams, J. Phys. II **5**, 1269 (1995).

[32] J. Lekner, Physica A **176**, 524 (1991).

[33] M. Daoud and J. P. Cotton, J. Phys. (France) **43**, 531 (1982).

[34] P. Guenoun, F. Muller, M. Delsanti, L. Auvray, Y. J. Chen, J. W. Mays, and M. Tirell, Phys. Rev. Lett. **81**, 3872 (1998).

[35] The exponent γ, however, is not universal and does not have a direct meaning in the sense of renormalization theory. It is rather used here as a fit parameter.

[36] O. V. Borisov, J. Phys. II **6**, 1 (1996).

[37] J. Jiang, H. Liu, and Y. Hu, J. Chem. Phys. **110**, 4952 (1999).

[38] G. S. Manning, J. Chem. Phys. **51**, 924 (1969).

[39] T. Odijk and A. H. Houwaart, J. Polym. Sci., Polym. Phys. Ed. **16**, 627 (1978).

[40] M. Deserno, C. Holm, and S. May, Macromolecules **33**, 199 (2000).

[41] E. Yu. Kramarenko, A. R. Khokhlov, and K. Yoshikawa, Macromol. Theory Simul. **9**, 249 (2000).

[42] J.-P. Hansen and H. Löwen, Annu. Rev. Phys. Chem. **51**, 209 (2000).

[43] C. N. Likos, Phys. Rep. **348**, 267 (2001).

[44] Y. Levin and M. E. Fisher, Physica A **225**, 164 (1996).

[45] M. N. Tamashiro, Y. Levin, and M. Barbosa, Physica A **258**, 341 (1998).

[46] T. A. Witten and P. A. Pincus, Macromolecules **19**, 2509 (1986).

[47] C. N. Likos, H. Löwen, M. Watzlawek, B. Abbas, O. Jucknischke, J. Allgaier, and D. Richter, Phys. Rev. Lett. **80**, 4450 (1998).

[48] A. R. Denton (unpublished).

[49] M. Heinrich, M. Rawiso, J. G. Zilliox, P. Lesieur, and J. P. Simon, Eur. Phys. J. E **4**, 131 (2001).

[50] A. Lang, C. N. Likos, M. Watzlawek, and H. Löwen, J. Phys.: Condens. Matter **12**, 5087 (2000).

[51] C. N. Likos, A. Lang, M. Watzlawek, and H. Löwen, Phys. Rev. E **63**, 031206 (2001).

[52] A. A. Louis, P. G. Bolhuis, J.-P. Hansen, and E. J. Meijer, Phys. Rev. Lett. **85**, 2522 (2000).

[53] A. A. Louis, P. G. Bolhuis, and J.-P. Hansen, Phys. Rev. E **62**, 7961 (2000).

[54] C. N. Likos, M. Schmidt, H. Löwen, M. Ballauff, D. Pötschke, and P. Lindner, Macromolecules **34**, 2914 (2001).

[55] A. A. Louis, Philos. Trans. R. Soc. London, Ser. A **359**, 939 (2001).

[56] A. J. Archer and R. Evans, Phys. Rev. E **64**, 041501 (2001).

[57] A. J. Archer and R. Evans, J. Phys.: Condens. Matter **14**, 1131 (2002).

[58] C. N. Likos and H. M. Harreis, Condens. Matter Phys. , (2002), in press.

[59] M. Watzlawek, H. Löwen, and C. N. Likos, J. Phys.: Condens. Matter **10**, 8189 (1998).

[60] M. Watzlawek, C. N. Likos, and H. Löwen, Phys. Rev. Lett. **82**, 5289 (1999).

[61] P. Ziherl and R. D. Kamien, Phys. Rev. Lett. **85**, 3528 (2000).

[62] P. Ziherl and R. D. Kamien, J. Phys. Chem. B **105**, 10147 (2001).

[63] M. Dijkstra, J. M. Brader, and R. Evans, J. Phys.: Condens. Matter **11**, 10079 (1999).

[64] C. von Ferber, A. Jusufi, M. Watzlawek, C. N. Likos, and H. Löwen, Phys. Rev. E **62**, 6949 (2000).

[65] C. von Ferber, A. Jusufi, C. N. Likos, H. Löwen, and M. Watzlawek, Eur. Phys. J. E **2**, 311 (2000).

[66] X. Guo and M. Ballauff, Phys. Rev. E **64**, 051406 (2001).

[67] J. D. Jackson, *Classical Electrodynamics*, 2nd ed. (Wiley, New York, 1975), p. 93.

[68] W. K. H. Panofsky and M. Phillips, *Classical Electricity and Magnetism*, 2nd ed. (Addison-Wesley, Reading, MA, 1962), p. 87.